MARMARA UNIVERSITY

INSTITUTE FOR GRADUATE STUDIES IN PURE AND APPLIED SCIENCES

EXPERIMENTAL INVESTIGATION OF MICROALGAE PYROLYSIS: KINETICS, THERMODYNAMICS, AND PRODUCT CHARACTERIZATION

ÖMER FARUK KILIÇ

MASTER THESIS

Department of Chemical Engineering

Thesis Supervisor
Assoc. Prof. Dr. Sevgi POLAT

Thesis CO- Supervisor
Prof. Dr. Perviz SAYAN

ISTANBUL, 2025

MARMARA UNIVERSITY

INSTITUTE FOR GRADUATE STUDIES IN PURE AND APPLIED SCIENCES

EXPERIMENTAL INVESTIGATION OF MICROALGAE PYROLYSIS: KINETICS, THERMODYNAMICS, AND PRODUCT CHARACTERIZATION

ÖMER FARUK KILIÇ

524523002

MASTER THESIS

Department of Chemical Engineering

Thesis Supervisor
Assoc. Prof. Dr. Sevgi POLAT

Thesis CO- Supervisor
Prof. Dr. Perviz SAYAN

ISTANBUL, 2025

ACKNOWLEDEGEMENTS

First of all, I would like to express my deepest gratitude to my advisor, Assoc. Prof. Dr. Sevgi Polat for her insightful guidance, support, and patience throughout my thesis.

Then, I would like to thank the Scientific and Technological Research Council of Turkey (TÜBİTAK-Project No. 224M617) and the Marmara University Scientific Research Projects Commission (Project No. FYL-2024-11408) for financially supporting this thesis.

I would like to acknowledge my dear and long-lasting friends Ahmet Tarık Akpınar and Rabia Altungöller, who have always stood by me without hesitation, strengthening me with their presence through my hardships.

My heartfelt thanks go to the esteemed YODA team and their members, who have allowed me to pursue my interests and advance in this field. Lastly, my deepest thanks to my dear friends Alperen Bulgur and Hale Ahsen Babar for their emotional camaraderie and collaborative spirit during this project.

Finally, to my family: my mother Lorna Lizza Menor, my father Haki Kılıç, my wife Sümeyra Aksoy Kılıç, and my dear brother Ahmed E. B. Kılıç, who have always been by my side, offering their love, support, and emotional support throughout my life. I am indebted to them for the encouragement to explore my ideas and the steady hand that kept the research focused and on track.

November-2025 **Ömer Faruk Kılıç**

CONTENTS

ACKNOWLEDEGEMENTS ..... **i**

CONTENTS ..... **ii**

ÖZET ..... **v**

ABSTRACT ..... **v**

SYMBOLS ..... **v**

ABBREVIATIONS ..... **vii**

LIST OF FIGURES ..... **vii**

LIST OF TABLES ..... **x**

1. INTRODUCTION **1**

1.1. The Purpose of the Study 1

1.2. Energy 2

1.3. Biomass 5

1.3.1. Types of Biomass 6

1.3.2. Microalgae 7

1.3.3. *Chlorella vulgaris* 8

1.4. Thermochemical Conversion Processes 10

1.4.1. Combustion 11

1.4.2. Liquefaction 11

1.4.3. Gasification 11

1.4.4. Pyrolysis 12

1.5. Experimental Design 13

2. MATERIALS AND METHOD **15**

2.1. Features of the microalgae 15

2.2. TGA-FTIR-MS analyses 15

2.3. Pyrolysis-GC/MS experimental procedure 16
2.4. Fixed-bed prolysis experiments 16
2.5. Characterization 19
2.6. Kinetic and Thermodynamic Modelling 20
3. RESULTS AND DISCUSSION 23
3.1. Characteristics of *Chlorella vulgaris* 23
3.2. Morphological characterization. 24
3.3. Structural characterization. 25
3.4. Thermal decomposition behavior of *Chlorella vulgaris* 31
3.5. Kinetics and thermodynamic analysis of *Chlorella vulgaris* 34
3.6. TGA/FTIR/MS analysis of *Chlorella vulgaris* 41
3.7. Py-GC/MS analysis of *Chlorella vulgaris* 43
3.8. Experimental design results. 45
3.9. Elemental composition of bio-oil 49
4. CONCLUSIONS 50
REFERENCES 51
LIST OF PUBLICATIONS ABOUT THE THESIS SUBJECT BEING PREPARED 61

ÖZET

MİKROALG PİROLİZİNİN DENEYSEL YÖNTEMLE İNCELEMESİ: KİNETİK, TERMODİNAMİK VE ÜRÜN KARAKTERİZASYONU

Fosil yakıtların tükenmesi ve artan çevresel problemler, sürdürülebilir enerji kaynaklarının arayışını hızlandırmıştır. Özellikle *Chlorella vulgaris* gibi mikroalgler; hızlı büyüme, yüksek fotosentetik verim ve zengin biyokimyasal bileşimleriyle biyoyakıt üretimi için umut verici biyokütle kaynaklarıdır. Bu tez çalışması kapsamında, *C. vulgaris*'in piroliz süreci detaylı olarak incelenmiş, termal bozunma davranışı, kinetik parametreleri ve sürdürülebilir enerji ürünleri olan biyochar ile biyoyakıt üretim potansiyeli değerlendirilmiştir. Termogravimetrik analiz sonuçları, aktif piroliz işleminin 200–500 °C aralığında gerçekleştiğini ve bu sıcaklık aralığında önemli miktarda uçucu bileşiklerin açığa çıktığını göstermiştir. Analiz sonuçları, elde edilen biyocharın belirgin şekilde artmış karbon içeriğine (%80,8), geniş yüzey alanına (161,3 m^2/g) ve yüksek ısıl değere (31,6 MJ/kg) sahip olduğunu göstermiştir. Flynn–Wall–Ozawa, Kissinger–Akahira–Sunose, Starink ve Tang gibi model-free yöntemlerle kullanılarak yapılan hesaplamalar sonucunda ortalama aktivasyon enerjisi 140 kJ/mol olarak hesaplanmıştır. Termodinamik değerlendirmeler, sürecin endotermik ve kendiliğinden gerçekleşmeyen bir yapıda olduğunu göstermiştir. TGA-FTIR-MS analizi sonucunda başlıca gaz ürünler CO_2, H_2O ve CH_4 olarak belirlenmiştir. Box–Behnken deney tasarımı optimizasyonu sonucunda, biyoyakıt verimini artırmada en etkili parametrenin ısıtma hızı olduğu tespit edilmiş ve optimum koşullar altında sıvı ürün verimi %32,08 olarak elde edilmiştir.

Anahtar kelimeler: *Chlorella vulgaris*, piroliz, TGA-FTIR-MS, model-free yöntemi, Box–Behnken tasarımı.

ABSTRACT

EXPERIMENTAL INVESTIGATION OF MICROALGAE PYROLYSIS: KINETICS, THERMODYNAMICS, AND PRODUCT CHARACTERIZATION

The search for renewable energy sources is growing as fossil fuels run out and environmental problems become more prominent. Microalgae, especially *Chlorella vulgaris*, are great sources of biomass for making biofuels because they grow quickly, photosynthesize better, and have complex metabolic systems. This thesis performed an extensive analysis of the pyrolysis process of *C. vulgaris*, evaluating its thermal degradation properties, kinetic parameters, and the potential of biochar and bio-oil as sustainable energy sources. Thermogravimetric analysis indicates that active pyrolysis occurs between 200 and 500 °C, during which several volatile compounds are released. The investigation revealed that the biochar contains a significant carbon content (80.8%), an extensive surface area (161.3 m^2/g), and an elevated calorific value (31.6 MJ/kg). The average activation energy was determined to be ~140 kJ/mol using model-free techniques, specifically the Flynn–Wall–Ozawa, Kissinger–Akahira–Sunose, Starink, and Tang methods. Thermodynamic assessments demonstrated that the process was endothermic and non-spontaneous. Gaseous products such as CO_2, H_2O, and CH_4 were identified via TGA-FTIR-MS. Process optimization using the Box–Behnken design identified heating rate as the most influential factor for maximizing bio-oil yield, achieving a maximum yield of 32.08 wt% under optimal conditions. In conclusion, the present study suggested that C. vulgaris appeared to be a promising renewable biomass for biofuel production using pyrolysis technology.

Keywords: *Chlorella vulgaris*, pyrolysis, TGA-FTIR-MS, model-free kinetics, Box–Behnken design.

SYMBOLS

A **:** Pre-exponential factor or frequency factor (min^{-1})

E **:** Activation energy (kJ/mol)

f(x) **:** Reaction model

g(x) **:** Integrated form of the reaction model

k(T) **:** Reaction rate constant

n : Reaction order

R **:** Ideal gas constant (8.314 J/mol.K)

T **:** Absolute temperature (K)

x **:** Conversion

β : Heating rate (°C/min)

ΔG : Gibbs free energy change (kJ/mol)

ΔH : Enthalpy change (kJ/mol)

ΔS : Entropy change (J/mol.K)

ABBREVATIONS

ASTM	**:** American Society for Testing and Materials
BBD	**:** Box–Behnken design
BET	**:** Brunauer-Emmett-Teller
DCM	**:** Dichloromethane
DTG	**:** Differential thermogravimetric
FTIR	**:** Fourier transform infrared higher heating value
HHV	**:** Higher heating value
FWO	**:** Flynn–Wall–Ozawa
KAS	**:** Kissinger–Akahira–Sunose
MS	**:** Mass spectrometry
Py-GC/MS	**:** Pyrolysis–Gas Chromatography/Mass Spectrometry
RSM	**:** Response surface methodology
SEM	**:** Scanning electron microscopy
TGA	**:** Thermogravimetric analysis
UN	**:** United Nations
XRD	**:** X-ray diffraction

LIST OF FIGURES

Figure 1.1. Renewable energy sources [33].....3

Figure 1.2. A schematic illustration of the cellular architecture of Chlorella species utilized in bioenergy research 9

Figure 1.3. Overview of the principal biomass conversion processes and their corresponding end products.....10

Figure 2.1. TGA-FTIR-MS system 15

Figure 2.2. Pyrolysis set-up system 17

Figure 3.1. SEM image and corresponding EDS spectrum of (a) raw Chlorella vulgaris, and (b) biochar obtained after pyrolysis at different magnification levels...26

Figure 3.2. FE-SEM elemental mapping images of raw *Chlorella vulgaris* 28

Figure 3.3. FE-SEM elemental mapping images of Chlorella vulgaris-derived biochar after pyrolysis 29

Figure 3.4. X-ray diffraction (XRD) patterns of *Chlorella vulgaris* before and after pyrolysis.....29

Figure 3.5. Fourier-transform infrared (FTIR) spectra of *Chlorella vulgaris* before and after pyrolysis 31

Figure 3.6. (a) TGA and (b) DTG curves; (c) conversion versus temperature profiles at different heating rates; (d) changes in activation energy (E, kJ/mol) in connection with the degree of conversion during the thermal decomposition of *Chlorella vulgaris.* 33

Figure 3.7. (a) ΔH, (b) ΔG, and (c) ΔS values obtained using the FWO model at different heating rates 36

Figure 3.8. (a) ΔH, (b) ΔG, and (c) ΔS values obtained using the KAS model at different heating rates. 37

Figure 3.9. (a) ΔH, (b) ΔG, and (c) ΔS values obtained using the Straink model at different heating rates 38

Figure 3.10. (a) ΔH, (b) ΔG, and (c) ΔS values obtained using the Tang model at different heating rates 39

Figure 3.11. Isoconversional plots for the pyrolysis of *Chlorella vulgaris* obtained using different model-free methods: (a) Flynn–Wall–Ozawa (FWO), (b) Kissinger–Akahira–Sunose (KAS), (c) Starink, and (d) Tang methods, at various conversion levels (α = 0.1–0.9) 40

Figure 3.12. (a) Gram–Schmidt curve; (b) three-dimensional (3D) FTIR spectrum; (c) selected absorbance intensities at characteristic wavenumbers over time for volatile species evolved from *Chlorella vulgaris*; (d) single ion current curves (m/z = 16, 18, and 44) for major gaseous products detected during the pyrolysis of *Chlorella vulgaris.* 42

Figure 3.13. Py-GC/MS analysis of volatile product classes obtained from the pyrolysis of *Chlorella vulgaris*. 44

Figure 3.14. (a) Perturbation plots. (b) Predicted vs. actual values of bio-oil yield. (c–e) 3D response surface and contour plots showing the interactions between (c) temperature and heating rate, (d) temperature and nitrogen flow rate, and (e) heating rate and nitrogen flow rate. 48

LIST OF TABLES

Table 1.1. Principal categories of biomass and their classification [45]. 7

Table 2.1. Coded levels of independent variables used in the Box–Behnken design for pyrolysis of *Chlorella vulgaris*.....18

Table 2.2. Experimental design matrix based on the Box–Behnken design.....19

Table 2.3. Kinetic models and their corresponding equations used in this study.....21

Table 3.1. Results of the proximate and ultimate analysis. 24

Table 3.2. Nitrogen adsorption data and BET surface area parameters for raw *Chlorella vulgaris* determined at 77 K using the BET method 27

Table 3.3. Nitrogen adsorption data and BET surface area parameters for biochar derived from *Chlorella vulgaris*, measured at 77 K using the BET method.....27

Table 3.4. Thermal decomposition characteristics of *Chlorella vulgaris* at the active pyrolysis region. 32

Table 3.5. Activation energies (E, kJ/mol) with respect to conversion degrees for pyrolysis of *Chlorella vulgaris*.....34

Table 3.6. Thermodynamic parameters at 20 °C/min using FWO and KAS models. 35

Table 3.7. Thermodynamic parameters at 20 °C/using Starink and Tang models. 35

Table 3.8. Experimental design matrix and corresponding bio-oil yields based on the Box–Behnken design. 45

Table 3.9. The results of the analysis of variance (ANOVA) for the quadratic model. 46

1. INTRODUCTION

1.1. The Purpose of the Study

From the beginning of time, people have needed energy to stay alive and grow. The more people there are on the globe, the more energy they use [1]. We need to find new and long-lasting sources of energy right away since the need for energy is rising, fossil fuel supplies are running out, and climate change is becoming a bigger concern. Also, fossil fuels are the main source of energy for combustion, which is bad for the health and environment of plants and animals. For example, they can cause respiratory problems and early deaths in people [2]. The need for energy is expanding faster than the United Nations and other international organizations can keep up with their efforts to make energy use more efficient and urge people to save energy [3]. This developing difference shows how important it is to make the transition to energy systems that are better for the environment.

Examples of renewable energy sources that come from things that can be naturally recycled are solar radiation, wind, geothermal activity, hydropower, and other types of biomass. These sources are currently a key part of the world's move to renewable energy sources [4,5]. Biomass energy is the most interesting, as it gives us a long-term source of energy that doesn't change how we farm or use land. Some countries don't have a lot of fossil fuels, thus they have to get most of their energy from other countries [6]. But traditional agricultural biomass isn't always adequate to supply the energy needs of large groups of people. This is especially true when you consider how much land is available and when it is accessible. That's why more and more people are looking at other types of biomass feedstocks that are beneficial for the environment and use resources well. Microalgae are one of the most important ones [7]. They are great for making bioenergy because they grow quickly, can use wastewater, and are good at fixing CO_2 [7,8]. *Chlorella vulgaris* (*C. vulgaris*) has attracted significant research interest due to its rapid growth, resilience, and biochemical versatility among the several species studied. Depending on how it is produced, *C. vulgaris* can store up to 50% of its dry weight in carbohydrates, proteins, or lipids [9].

C. vulgaris has a lot of potential for thermochemical processing methods, especially pyrolysis. Recent advancements indicate that pyrolysis could function as an effective thermochemical method for converting microalgal biomass into energy-rich molecules [10–12]. Thermogravimetric analysis (TGA) is a crucial tool for the investigation of biomass pyrolysis, as it measures weight loss and thermal behavior during regulated heating [13]. TGA-based investigations employ iso-conversional and model-fitting methodologies to extract kinetic and thermodynamic characteristics, such as activation energy and pre-exponential factors [14]. Thermogravimetric analysis (TGA) combined with FT-IR and MS can reveal gas-phase products [15,16].

This thesis offers an extensive thermal investigation of *C. vulgaris* to clarify its pyrolytic properties. We looked at important factors like kinetic behavior, degradation phases, and product yields to identify a strategy to help make successful and circular energy recovery methods that use microalgal feedstocks. The Box–Behnken (BBD) design, a response surface method that estimates how different operational factors would affect each other, was also utilized to statistically optimize process variables that affect pyrolysis efficiency and bio-oil yield. This method helps us understand the process better and makes it easier to determine the ideal pyrolysis conditions for energy applications that can be expanded.

1.2. Energy

There are many things that people need to live and improve their lives. Housing, heating, food, transportation, and entertainment are some of these. Most of these things require a constant supply of energy. Throughout history, society and technology have changed in ways that have always made this energy demand grow. As a result, people have tried to get energy from many different sources. Energy sources are usually divided into two groups: renewable and non-renewable. This is based on how easily they can be replaced in nature [17].

Natural geological and biological processes have generated the materials needed to make non-renewable energy sources over millions of years. They are called non-renewable because they consume resources quickly than they can be replaced. Some examples of resources that are often found deep in the ground are coal, crude oil, natural gas, and petroleum. Taking them out affects the ecosystem a lot of the time [18].

Burning these minerals for energy releases nitrogen oxides (NO_x), sulfur oxides (SO_x), and carbon oxides (CO_x). These molecules build up in the atmosphere, which destroys important biological processes like the carbon and nitrogen cycles. This makes the greenhouse effect stronger and speeds up global warming [19–22].

Global warming is an enormous risk to people because it disrupts the Earth's natural balance. That's why it is a necessity to transition to renewable energy sources or, at a minimum, implement strategies that mitigate the risks associated with fossil fuel dependence [23]. Renewable energy, on the other hand, derives from processes that happen naturally on Earth and can be used more than once. Figure 1.1 shows that these types of energy include solar, wind, hydroelectric, geothermal, and biomass energy. These kinds of resources come from natural cycles, including solar radiation, the movement of air, and the water cycle.

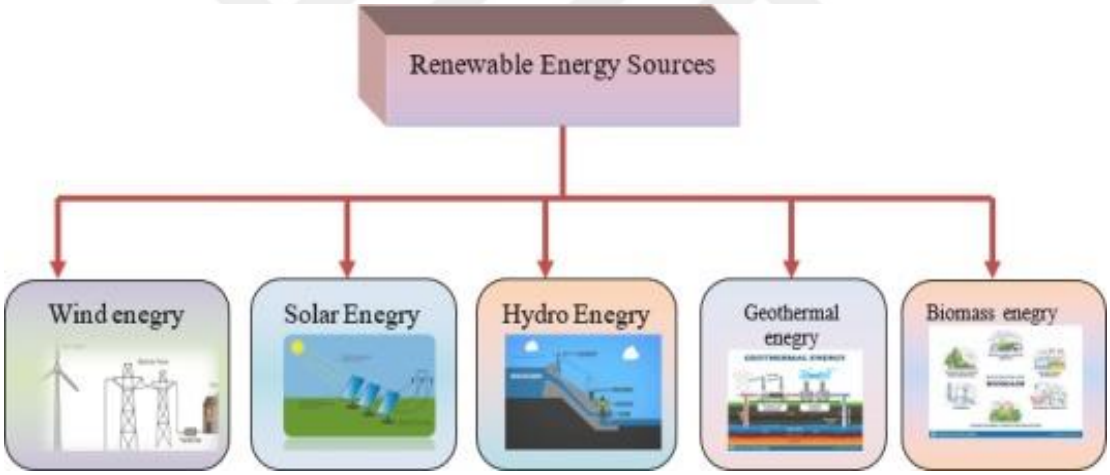

Figure 1.1. Renewable energy sources [24].

Renewable energy technologies turn these resources into electricity, heat, or mechanical power that people may utilize every day. Many countries are working hard to convert to renewable energy sources to lessen their impact on the environment and become more energy self-sufficient. The UN and other international groups want more countries to use renewable energy in their energy use. The United Nations wants the use of renewable energy around the world to quadruple by 2030 [24–26]. Renewable

technologies provide eco-friendly options, but each comes with its own set of technological, economic, and environmental issues.

Solar energy, which comes from the sun, is one of the oldest and most basic sources of energy. The Sun sends a lot of energy to Earth every year. A small amount of energy could easily meet the energy needs of the whole world several times over. Photovoltaic or thermal systems turn this energy into heat or electricity. Solar energy is plentiful, but because it changes throughout the day and year, it needs effective energy storage devices to make sure there is always enough [18]. Turkey has a lot of potential for solar energy because it gets a lot of sunlight every year, especially in the south and southeast.

Changes in atmospheric pressure that move air masses create wind energy, which is a plentiful and long-lasting renewable resource. After hydropower, this is the second most common way to create electricity from renewable sources. This is because it has new technology, is affordable, and is easy to get around. Turbines with horizontal or vertical axes change energy into mechanical or electrical forms without releasing any hazardous gases. Thanks to advances in technology, wind energy is now as affordable as fossil fuel systems. But climate change could modify the normal wind speeds, which could make wind energy less useful in the future. Studies reveal that results will vary from one place to another. There may be small drops or mild rises in some parts of Europe and Brazil, but there may be big drops in China and the northwestern United States, especially in the summer. These differences show how important it is to plan ahead and improve turbine technologies so that wind energy generation is always reliable [27–29].

Geothermal energy comes from the heat inside the Earth. It is a renewable resource that can supply the world's energy demands without harming the environment. This is because the middle of the Earth is hotter than the layers around it, which are cooler. This helps heat move to water sources that are below the surface. There aren't many geothermal reservoirs that can provide enough electricity, but geothermal energy is utilized a lot in greenhouses for farming, heating systems, and other industrial uses. Geothermal steam is employed to produce electricity, which can then energize

desalination plants in multiple ways. Notwithstanding its myriad advantages, geothermal energy is still less employed than other renewable resources [30].

Hydropower is made by turning the potential energy of water into electrical energy. The most common way to do this is by using hydroturbines, which are found in dams or reservoirs. It now provides more than 21% of the world's electricity and has a total installed capacity of over 1,000 GW. Hydropower projects are cost-effective and rather reliable, yet they can hurt local ecosystems and aquatic habitats. To lessen these effects, it is important to think about the long term and take steps to protect the ecosystem from these impacts [31].

Biomass energy is the use of organic materials like animal waste, wood, agricultural waste, oil-rich plants, sugar-rich plants, and municipal solid waste. Biomass is a renewable resource that comes from the area. It helps society and the economy move forward while using fewer fossil fuels. You can burn it right away, or you can turn it into better biofuels that can be used to make energy or help with transportation.

1.3. Biomass

Plants, algae, trees, and crops are examples of living things that make up biomass. Biomass is made up of chemical energy that comes from solar energy and is stored. This word refers to plants that do well in both water and land, as well as organic waste. Biomass has been an important source of energy for a long time and now meets about 10–14% of the world's energy needs [32].

Biomass is a renewable energy source that has several benefits that other sources don't have. For example, it can make solid, liquid, and gaseous fuels, which sets it apart from many other renewable sources that just provide heat or power. It could help a lot with energy problems like running out of fossil fuels and producing greenhouse gases. When biomass is made in ways that don't harm the environment, the carbon dioxide that comes out of it when it is turned into something else is almost the same as the carbon dioxide that goes into it while it grows. That means it doesn't release any carbon into the air. Biochemical and thermochemical methods can turn biomass into fuels that can be sold instead of fossil fuels [33].

The type of biomass employed for energy production depends on its distinct characteristics, the desired fuel type, and the intended conversion method. The primary factors constituting bulk density include moisture content, calorific value, fixed carbon and volatile matter quantities, ash and alkali metal content, and the cellulose to lignin ratio. Hemicellulose, cellulose, lignin, and other organic materials that break down at different rates make up most of the biomass. Hemicellulose is a polymer made up of multiple polysaccharides that doesn't have a specific form. It quickly turns into gases, including carbon monoxide, carbon dioxide, and hydrocarbons. Cellulose is a strong crystalline polymer made of glucose that doesn't change much when the temperature rises. Lignin, on the other hand, is a highly branched aromatic polymer with a complex structure that affects how it breaks down [34,35].

1.3.1. Types of Biomass

Table 1.1 shows that biomass comes from many different places and can be put into different groups based on where it comes from. The European Committee for Standardization (EN 14961, EN 15234) says that biomass can be divided into four primary groups: woody, herbaceous, fruit biomass, and combinations or blends. Woody biomass is made up of trees, shrubs, and bushes, but not their seeds or fruits. Plants that exist for only one growing season, such as grains and cereals, make up herbaceous biomass. Fruits are botanically part of woody plants, even though they are often thought of as independent things. Mixtures happen by accident, but blends are planned mixes of different types of biomasses. Biomass is a broad term that includes all plant materials and animal waste. It may be broken down into two main types: virgin (primary) biomass, which comes straight from plants or animals, and waste (derived) biomass, which includes leftovers and by-products. Virgin biomass is mostly made up of lignocellulosic materials like wood and leaves, as well as crops that are high in carbohydrates. trash biomass is made up of organic materials such as municipal trash, sewage sludge, animal and human waste, gases that come from landfills, and agricultural waste [36].

Table 1.1. Principal categories of biomass and their classification [36].

A.Virgin Biomass	A.1 Terrestrial biomass	i. Forest biomass ii. Grasses iii. Energy crops iv. Cultivated crops
	A.2 Aquatic biomass	i. Algae ii. Water plant
B. Waste biomass	B.1 Municipal waste	i. MSW ii. Biosolids, sewage iii. Landfill gas
	B.2 Agricultural solid waste	i. Livestock and manures ii. Agricultural crop residue
	B.3 Forestry residues	i. Bark, leaves, floor residues
	B.4 Industrial wastes	i. Demolition wood, sawdust ii. Waste oil/fat

1.3.2. Microalgae

Algae are a big, varied, and diversified category of photosynthetic organisms that come from several evolutionary lineages. There are both eukaryotic and prokaryotic forms, and they come in a wide range of sizes and shapes. Some are single-celled organisms that are only a few micrometers in diameter, while others are sophisticated multicellular seaweeds that can grow to be several meters long. Algae live in practically all bodies of water, both freshwater and saltwater, and they are an important part of the world's carbon and oxygen cycles. These creatures use photosynthesis to turn carbon

dioxide and water into organic matter, releasing oxygen in the process. This makes them the base of many aquatic food chains [37].

Algae are primarily categorized into two types: macroalgae and microalgae. This is determined by their morphology and cellular architecture. Seaweeds, or macroalgae, are multicellular organisms visible to the naked eye. They are divided into three families based on the color of their pigments: red (*Rhodophyceae*), green (*Chlorophyceae*), and brown (*Phaeophyceae*). Microalgae are little organisms that are mostly made up of one cell. They can live by themselves or with a few colonies. The biochemical composition of microalgae differs based on the strain and cultivation method. It normally comprises 30–55% protein, 15–25% carbohydrates, and 15–30% lipids when dried. They also have minor amounts of minerals like calcium, potassium, iron, and sulfur, as well as some unsaturated fatty acids. Some kinds of microalgae have a lot of lipids, which makes them great for creating biofuels and other things that are useful [38,39].

Microalgae are simple, photosynthetic microorganisms that may grow swiftly in saltwater, freshwater, or even wastewater by using sunlight and CO_2 from the air. They are a green alternative source of renewable fuel since they grow quickly, store a lot of carbon, and don't need much area or freshwater. Microalgae-based biofuels also have little or no sulfur, which means they pollute less than fossil fuels. Microalgae can do more than just provide us with energy. The biochemical portions of these foods, such as colors, vitamins, and fatty acids, are also used in the food, beauty, and drug sectors. Using a microalgal biorefinery technique to create biofuels and these high-value items at the same time is excellent for both the economy and the environment [40,41].

1.3.3. *Chlorella vulgaris*

Chlorella vulgaris is a type of green microalga that has only one cell. It belongs to the Chlorophyta category. They are normally 2 to 10 μm broad and don't have any flagella. This kind of plant is great at photosynthesis and can grow well in many different places. In 1890, Martinus Beijerinck was the first person to write about this eukaryotic species. It is known for being able to photosynthesize swiftly and live in a

wide range of places. *C. vulgaris* needs large amounts of carbon, nitrogen, and phosphorus, as well as modest amounts of minerals, to grow well. It grows best when the temperature is between 25 and 30 °C and the pH is between 6.5 and 9. It can use light well since it has chloroplasts full of chlorophyll and b. The robust, thick cell wall protects it and keeps it stable [40,42].

C. vulgaris is made up of 50–60% proteins, 12–30% carbs, and 4–22% lipids. There are several micronutrients in it, such as vitamins (B-complex, C, D, folic acid, α-tocopherol), minerals (iron, potassium, calcium, phosphorus, magnesium), and pigments (lutein, β-carotene, astaxanthin, canthaxanthin). *Chlorella* has a lot of different compounds in it; therefore, it is utilized in aquaculture, medicine, nutrition, and generating biofuels [40,43]. The cell wall of *Chlorella* alters as it grows. Immature cells have only one thin layer, but mature cells have two or three layers with thick outer coats. Cellulose and hemicellulose make up most of the inner microfibrillar layer, which makes it strong. The outside layer is made up of proteins and carbohydrates. The structural characteristics determine how easily intracellular molecules can get to one another, which in turn affects how well bioenergy conversion activities work [40,43]. Figure 1.2 provides a diagram of the cell structure of Chlorella as it relates to bioenergy usage. It highlights the main components of the structure that make it an excellent choice for a bioresource that will survive for a long time.

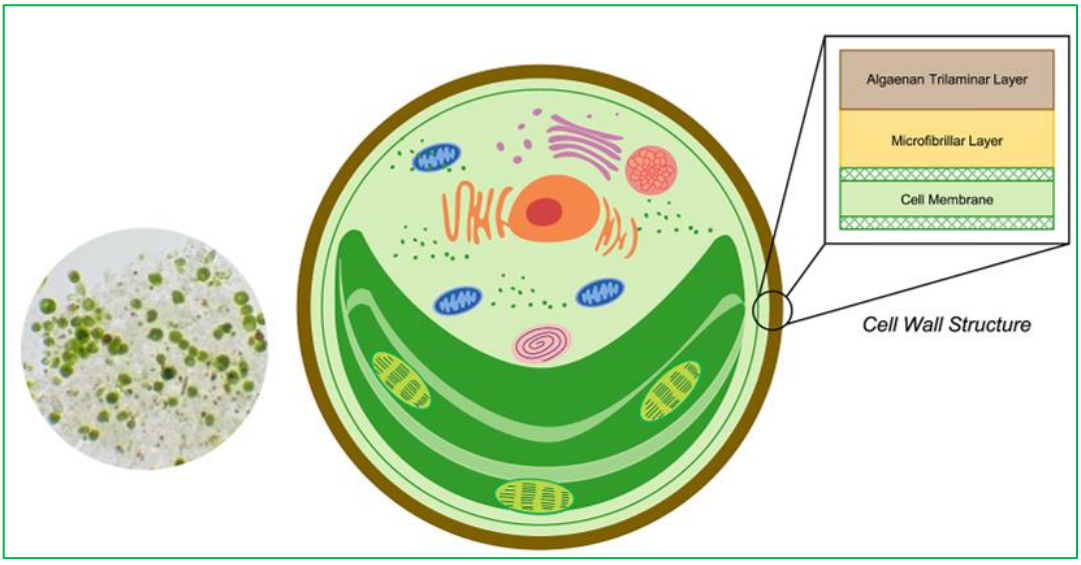

Figure 1.2. A schematic illustration of the cellular architecture of *Chlorella* species utilized in bioenergy research [40].

1.4. Thermochemical Conversion Processes

Several technological approaches are utilized to transform biomass into solid, liquid, or gaseous fuels for energy generation. Figure 1.3 depicts how different types of biomass, how they are turned into fuels, and how they are used are all linked. Biomass can be modified in three basic ways: thermochemical, biochemical, and physicochemical [44,45].

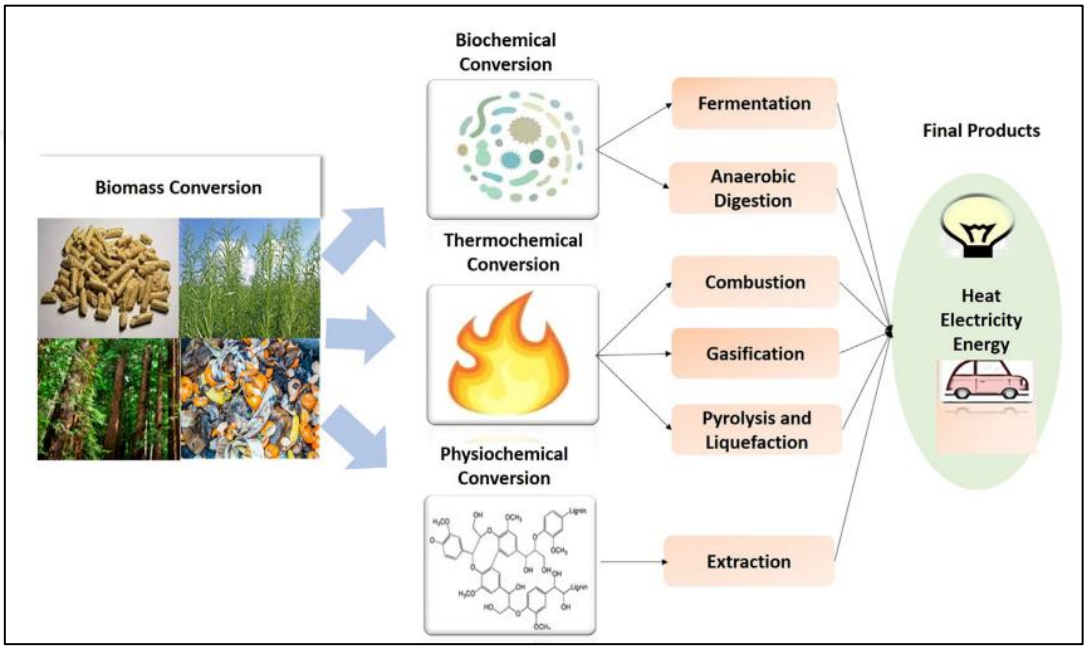

Figure 1.3. Overview of the principal biomass conversion processes and their corresponding end products [45].

Biomass can be turned into valuable chemicals and different kinds of energy in several ways. The three basic types of conversion processes are thermochemical, biological, and physicochemical. Thermochemical processes, such as combustion, gasification, pyrolysis, and liquefaction, use heat to generate energy carriers or products that can be used in other processes. Biochemical conversions turn things into biogas by aerobic digestion and bioalcohols like ethanol by fermentation. The physicochemical pathway is the means to extract lipids from a substance so that biodiesel can be made. These steps let you manufacture chemicals and fuels that are good for business and easy

to transfer, store, and utilize. The quality and makeup of biomass-based fuels depend a lot on the type of biomass and how it is transformed into fuel [46,47].

1.4.1. Combustion

Combustion is the most prevalent thermochemical conversion process. It happens when something burns and releases the chemical energy it has stored. Boilers, furnaces, turbines, and generators use the heat that is made to make thermal and electrical energy. Boilers, furnaces, turbines, and generators use the heat that comes from this to make thermal and electrical energy. The process normally happens between 800 and 1000 °C, which creates gases that can be used to make energy. The way biomass is made and how much water it has in it have a big effect on how well it burns.

Biomass has more water and oxygen and less carbon than coal. This means that it doesn't burn as well, but it is more reactive and less stable. Alkali metals, silica, and chlorine are some examples of inorganic substances that can foul up combustion systems and cause slagging. Even with these problems, biomass is still a cheap, carbon-neutral, and promising renewable fuel that can create power for a long time [48].

1.4.2. Liquefaction

Biomass liquefaction is a pioneering thermochemical process that turns biomass into useful products like bio-oil (40–60%), charcoal (10–12%), and gases (35–45%). The procedure usually takes place in solvents like water, ethanol, or tetralin at high pressures (5–25 MPa) and moderate temperatures (200–600°C). The parameters of the method have a considerable impact on both the amount and the quality of the product. Cellulose and hemicellulose make up biomass. These are particularly important since they break down more quickly. This is because their structures are simpler, and they break down at lower temperatures. In addition to components of biomass, temperature and pressure play a vital role in the liquefaction process to improve the bio-oil yield. [49–51].

1.4.3. Gasification

Gasification is a thermochemical conversion process that uses partial oxidation at temperatures typically higher than 600 °C to convert biomass into a flammable gas mixture known as synthesis gas (syngas). When air is used as the gasifying medium,

the process typically occurs in three stages: drying, pyrolysis, and oxidation. The end product is a mixture of carbon monoxide, carbon dioxide, hydrogen, methane, and nitrogen. On the other side, steam gasification generates a gas that is less diluted since it has more hydrogen and heat value and less nitrogen. The kind of gasifying medium, the amount of moisture, the temperature of the reaction, and the qualities of the feedstock all have a big effect on the quality and make-up of syngas. Several people argue that air gasification is a better way to make energy on-site because it is cheap and easy to utilize. In situations where a lot of power is needed, steam gasification is better. Catalysts such as dolomite, nickel-based compounds, and alkali metals are frequently employed to produce a greater quantity of gas and minimize the production of creosote [50].

1.4.4. Pyrolysis

Pyrolysis is a thermochemical process that breaks down organic feedstocks, mainly biomass, using heat in an oxygen-free atmosphere. This change makes three main things: solid char, liquid bio-oil, and gases that can't transform into liquids. The reaction temperature, the speed at which the heat is applied, and how long the vapor stays in the air all have a big effect on how much of each product is made. The characteristics of the biomass feedstock significantly influence the quantity of product generated. The process of making biochar is usually slow pyrolysis. The process makes bio-oil and methane, which can be used to make energy and useful compounds, including acetone, methanol, and acetic acid. Compared to the pyrolysis, rapid or flash pyrolysis is performed at higher heating rates and shorter vapor residence times, resulting in an increase in bio-oil yields—typically up to 70–80 wt%, depending on the properties of the feedstock [52,53].

Pyrolysis breaks down biomass in several thermal stages. The first stage (below ~150 °C) is the drying phase, during which the moisture evaporates with little change to the chemicals. This shows up as a small mass loss on the TG curve. Unstable substances, such as certain hemicellulose and lignin, are degraded during the second phase, pre-pyrolysis (150–250 °C). Carbon monoxide, dioxide, and acetic acid are emitted. Amorphous cellulose particles also change in terms of shape. Most devolatilization occurs in the first 250–500 °C pyrolysis stage. The components are

turned into carbon-rich charcoal. Above 500 °C, other particles break down slowly, leaving a carbon-rich, long-lasting char. Biomass cellulose, hemicellulose, and lignin affect reaction heat and intensity [54].

It emits gases such as CO and CO_2, as well as light organics like acetic acid. Simultaneously, the amorphous sections of cellulose transform morphology. During the initial stage of pyrolysis, which occurs between 250 and 500 °C, a significant amount of devolatilization occurs. This generates gases and vapors that can be converted into liquids, including CO, CO_2, CH4, and H_2. The progressive disintegration phase commences when the temperature exceeds 500 °C. The substances that remain continue to decompose until they form a stable char that is rich in carbon. Above 500 °C, a slow degradation phase occurs as residual solids continue to decompose into a stable carbon-rich char. The temperature ranges and reaction intensities are dependent on the biomass's cellulose, hemicellulose, and lignin contents [54].

Depending on the heating rate and reaction duration, pyrolysis processes are typically classified as slow or fast (flash) pyrolysis. Slow pyrolysis is operated at relatively low heating rates and longer vapor residence times to maximize solid char yield, generally producing around 30–35% char and lower amounts of liquid products. The final temperature and the duration of solid–phase reactions significantly affect both the yield and the quality of the char obtained. Fast pyrolysis tries to make as much bio-oil as possible by quickly heating finely ground biomass—usually with particles smaller than 5 mm—to about 500 °C. To stop subsequent cracking or polymerization events that would lower the oil production, it is important to quickly remove and cool condensable vapors in a few seconds under these conditions. To ensure efficient heat transfer, the feedstock is normally dried to less than 10% moisture before processing [55].

1.5. Experimental Design

Experimental design is essential for process improvement because it allows researchers to methodically investigate the influence of different factors on a response variable. Statistical design of experiments enables a comprehensive analysis of multiple parameters and their interrelations, enhancing our understanding of process functionality compared to sequential modifications of individual factors. The Box–

Behnken Design (BBD) is a type of Response Surface Methodology (RSM) that is commonly employed because it is quick and accurate for fitting quadratic models with only a few runs. In the BBD structure, each independent variable has three coded values: −1, 0, and +1. Experimental points are set in the midpoints of the factor ranges, with some points being repeated. This arrangement allows for the estimation of both main and interaction effects without the necessity of conducting experiments at extreme factor levels. This saves money and cuts down on mistakes in experiments while keeping the model correct [56–60].

Within the scope of this thesis, Box-Behnken design technique was used to optimize bio-oil production in fixed-bed pyrolysis experiments. Each experiment was repeated twice to ensure consistency. The variables were given the labels -1, 0, and +1 to show low, medium, and high values. To demonstrate how process parameters affect bio-oil production, we fitted the data with a second-order polynomial regression model. Model adequacy was evaluated using analysis of variance (ANOVA). These statistical tools confirmed the model's reliability and predictive capability [61,62]. This optimization study helped us figure out how to obtain the maximum bio-oil from *C. vulgaris* and do fewer tests.

2. MATERIALS AND METHOD

2.1. Features of the microalgae

Chlorella vulgaris is purchased from the Haznedaroğlu Laboratory at Boğaziçi University in Istanbul. The purpose of this drying procedure was to get rid of as much moisture as possible from the *C. vulgaris*, which would make the pyrolysis process work better. The ASTM standards were used to do a proximate and ultimate analysis on this microalga.

2.2. TGA/FTIR/MS analyses

The pyrolytic behavior of *C. vulgaris* was investigated using TGA coupled with FTIR and MS to identify the volatile products evolved during decomposition. The schematic representation of the TGA-FTIR-MS system used in the analysis is presented in Figure 2.1. Pyrolysis of the microalgae sample using the TGA/FTIR/MS system was carried out by connecting the gas transfer lines of the TGA device with the FTIR spectrometer and mass spectrometer.

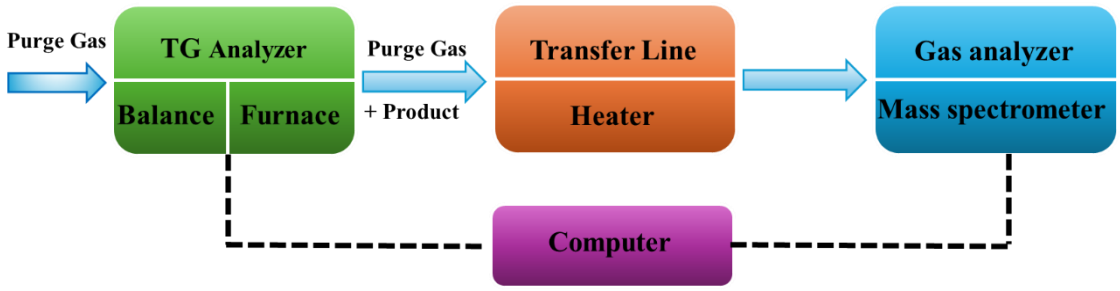

Figure 2.1. TGA-FTIR-MS system.

Thermal decomposition experiments were performed between 30 °C to 1000 ºC in the TGA. For this purpose, 20±0.5 mg samples were used, and they were heated using different heating rates of 10, 20, and 30 °C/min at a nitrogen flow rate of 100 ml/min. The transfer lines were heated throughout the experiment to prevent condensation of the gases released between the TGA and the FTIR/MS device. These temperatures were set as 220 °C for the TGA-FTIR system and 240 °C for TGA-MS. During the experiments,

FT-IR spectra were recorded in the wavelength range 400 to 4000 cm^{-1}, and three-dimensional graphs showing the changes in functional groups were obtained. Using the TGA/MS system, changes in the mass/charge (m/z) ratios of the gases formed during the experiment were recorded.

2.3. Py-GC/MS experiments

Py-GC/MS allows you to break down and identify volatile compounds at the same time, giving you an entire understanding of the composition of the liquid and gas fractions generated from biomass. This advanced analytical technique is often used to study the pyrolytic behavior of biomass because it is very sensitive and processes data quickly. A pyrolysis experiment was conducted in this study utilizing a Frontier Py-2020iS micro-pyrolyzer integrated with a Shimadzu QP2010 GC/MS system. In the microfurnace, about 1 mg of *C. vulgaris* sample was quickly pyrolyzed at 500 °C for 10 minutes in an inert atmosphere. The volatile compounds generated were promptly directed into the gas chromatograph for separation. Chromatographic separation was performed using a Frontier Ultra Alloy capillary column. Mass spectrometry detection utilized electron ionization (EI) at 70 eV, scanning a mass-to-charge (m/z) range from 20 to 200. Identification of pyrolysis products was carried out by comparing the acquired spectra with those in the NIST mass spectral database.

2.4. Fixed-bed pyrolysis experiments

Following the TGA-based thermal analysis, bench-scale pyrolysis experiments were performed using a fixed-bed reactor system. As illustrated in Figure 2.2, the experimental setup consists of a vertical tubular reactor constructed from stainless steel. A 10 g portion of air-dried microalgae sample was loaded into the reactor, and the system was purged with high-purity nitrogen (99.999%) prior to each run to ensure an inert atmosphere. Nitrogen was constantly supplied from the reactor's top during pyrolysis at a flow rate of 100 cm^3/min, which was controlled by a rotameter. Until the final pyrolysis temperature of 500 °C was attained, the heating was carried out at a steady rate of 10 °C/min.

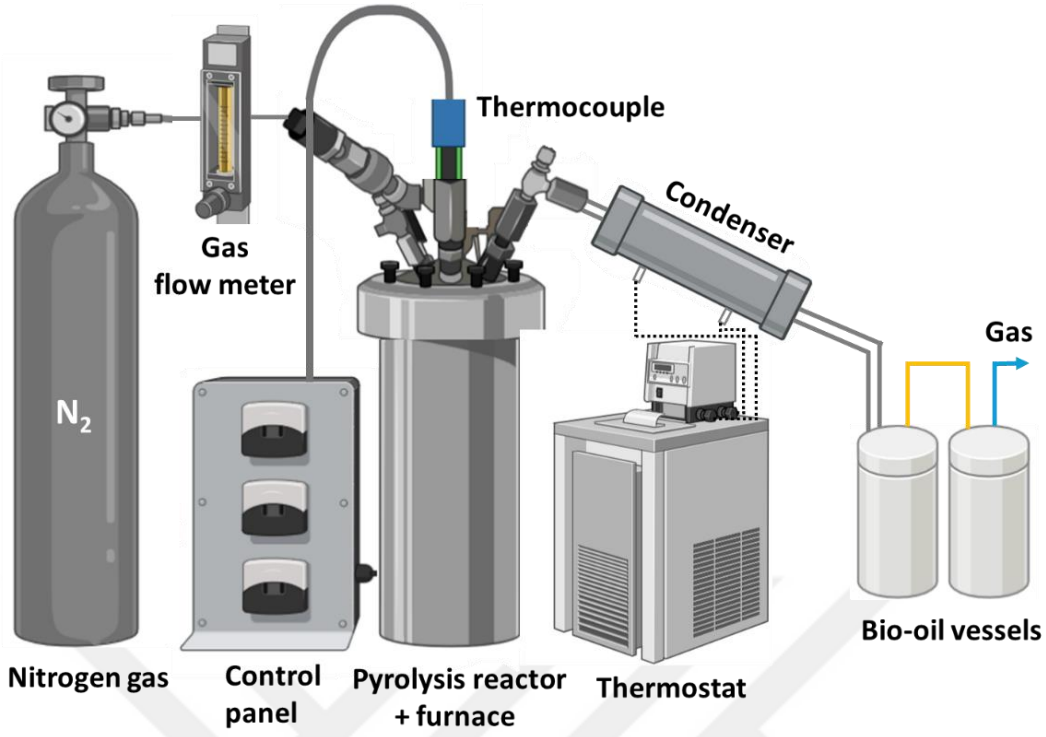

Figure 2.2. Pyrolysis set-up system.

The reactor outlet was connected to a thermostated condensation system that used a brine–ice mixture to keep the temperature close to 0°C in order to condense and collect the volatile products. Liquid fractions were captured as condensable vapors by using a sequence of traps. To recover any remaining organics, dichloromethane (DCM) was used to rinse these traps. At the end of each pyrolysis experiment, the remaining solid (char) mass inside the reactor was weighed to determine the mass. The pyrolysis liquid product, which accumulates in the collection vessel as a result of condensation, is removed by washing with DCM, and the resulting water fraction is separated using a separating funnel and then measured with a measuring cylinder. The liquid product is passed through sodium sulfate and dehydrated before being removed from its solvent in a rotary evaporator, and its yield is calculated. The non-condensable gaseous product yield under the cooling conditions applied throughout the experiment is calculated from the total mass balance. Each experiment was performed at least three times under the same operating conditions. These repeated experiments aim to increase the reliability and accuracy of the results.

This study also focused on enhancing important process parameters as well as the fixed-bed pyrolysis studies in order to maximize the production of bio-oil using the experimental design technique. A Box–Behnken Design (BBD) was applied through Design-Expert software to evaluate interactions between variables (pyrolysis temperature: A, heating rate: B, and nitrogen flow rate: C) and predict optimal operating conditions. The parameter ranges and coded levels used in the design are presented in Table 2.1, while the experimental combinations and corresponding bio-oil yields are listed in Table 2.2.

Table 2.1. Coded levels of independent variables used in the Box–Behnken design for pyrolysis of *Chlorella vulgaris*.

Design variable	**Symbol**	**Range and levels**		
		-1	0	1
Pyrolysis Temperature (°C)	A	400	500	600
Heating Rate (°C/min)	B	10	55	100
Nitrogen Gas Flow Rate (mL/min)	C	50	100	150

Table 2.2. Experimental design matrix based on the Box–Behnken design.

Run	Actual level of variables			Coded level of variables		
	Temperature	Heating Rate	Gas Flow Rate	A	B	C
1	500	10	50	0	-1	-1
2	500	100	50	0	+1	-1
3	500	10	150	0	-1	+1
4	500	100	150	0	+1	+1
5	400	10	100	-1	-1	0
6	400	100	100	-1	+1	0
7	600	10	100	+1	-1	0
8	600	100	100	+1	+1	0
9	400	55	50	-1	0	-1
10	400	55	150	-1	0	+1
11	600	55	50	+1	0	-1
12	600	55	150	+1	0	+1
13	500	55	100	0	0	0
14	500	55	100	0	0	0
15	500	55	100	0	0	0

2.5. Characterization

The structural analysis of *C. vulgaris* before and after pyrolysis was performed using XRD. Measurements were conducted at 40 kV and 30 mA over a 2θ range of 10° to 80°. Functional groups of the samples were identified using Fourier-transform infrared spectroscopy (FTIR) with an IR Affinity-1 spectrometer. Spectra were recorded in transmission mode at room temperature, within the wavenumber range of 650–4000 cm^{-1}. Morphological changes before and after pyrolysis were examined using a Scanning Electron Microscope with Energy Dispersive Spectroscopy. Surface area and porosity analysis were carried out using the BET (Brunauer–Emmett–Teller) method with a Micromeritics Asap 2020 analyzer, both before and after pyrolysis.

Elemental analysis of the solid residues and bio-oil samples was performed using a LECO CHNS 628 elemental analyzer.

2.6. Kinetic and thermodynamic modelling

Thermogravimetric analysis is widely utilized to investigate the thermal degradation behavior of solid materials and to extract critical kinetic parameters such as activation energy (E_a), pre-exponential factor (A), and reaction mechanism.

Equation 2.1 can be used to calculate the solid sample kinetic parameters during pyrolysis:

$$\frac{d\alpha}{dt} = k(T)\, f(\alpha) \tag{2.1}$$

Where α is the conversion degree, t is time, $k(T)$ is the temperature-dependent rate constant, and f(α) represents the reaction model. The conversion degree is calculated as:

$$\alpha = \frac{W_0 - W_t}{W_0 - W_f} \tag{2.2}$$

where W_0, W_t *and* W_f are initial, time-dependent, and final masses of the sample, respectively. The temperature-dependent rate constant $k(T)$ follows the Arrhenius equation:

$$k(T) = A\exp\left(-\frac{E}{RT}\right) \tag{2.3}$$

where A is the pre-exponential or frequency factor (min^{-1}), E is the activation energy (kJ/mol), T is the absolute temperature (K), and R is the ideal gas constant (8.314 J/mol K). Under a linear heating program, the heating rate (β=dT/dt) allows Equation (2.1) to be expressed as:

$$\frac{d\alpha}{dT} = k(T)\, f(\alpha) = \frac{A}{\beta}\exp(-\frac{E}{RT})\, f(\alpha) \tag{2.4}$$

Integration of Equation (2.4) yields:

$$\int_0^{\alpha} \frac{d\alpha}{f(\alpha)} = g(\alpha) = \frac{A}{\beta} \int_{T_0}^{T} \exp(-\frac{E}{RT})dT = \frac{AE}{\beta R} p(u) \tag{2.5}$$

where $p(u)$ and $g(\alpha)$ show the temperature integral and the integrated reaction model, respectively.

Since the integral on the right-hand side lacks an exact analytical solution, several iso-conversional (model-free) methods have been developed based on appropriate approximations of the temperature integral. In this study, four commonly used model-free methods—Flynn–Wall–Ozawa (FWO), Kissinger–Akahira–Sunose (KAS), Starink, and Tang—were employed to determine the apparent activation energy as a function of the conversion degree (α=0.1–0.9). The linearized forms of these methods and their respective plotting schemes are summarized in Table 2.3.

Table 2.3. Kinetic models and their corresponding equations used in this study.

Kinetic model	General model equations	Plotting method
FWO	$\ln \beta = \ln\left(\frac{AE}{Rg(x)}\right) - 5.331 - 1.052\frac{E}{RT}$	ln (β) vs (1/T) Slope= −1.052E/R
KAS	$\ln\left(\frac{\beta}{T^2}\right) = \ln\left(\frac{AR}{Eg(x)}\right) - \frac{E}{RT}$	ln (β/T^2) vs (1/T) Slope= −E/R
Starink	$\ln\left(\frac{\beta}{T^{1.92}}\right) = C - 1.0008\frac{E}{RT}$	ln (β/$T^{1.92}$) vs (1/T) Slope= −1.0008E/R
Tang	$\ln\left(\frac{\beta}{T^{1.8947}}\right) = C - 1.00145\frac{E}{RT}$	ln (β/$T^{1.8947}$) vs (1/T) Slope= −1.00145E/R

The frequency factor (A) for each conversion level was calculated using a modified Kissinger equation:

$$A = \frac{\beta E \exp(E / RT_{peak})}{RT_{peak}^2} \tag{2.6}$$

where T_{peak} is the peak temperature of the derivative thermogravimetric (DTG) curve.

Determining thermodynamic parameters is an essential stage in understanding more about biomass pyrolysis. Determining the thermodynamic properties makes it easier to calculate the energy needed for the pyrolysis process and assess the feasibility of the method. Following the determination of enthalpy change (ΔH), Gibbs free energy change (ΔG), and entropy change (ΔS) were estimated using Equations 2.7-2.9.

$$\Delta H = E - RT \tag{2.7}$$

$$\Delta G = E + RT_{peak} \ln\left(\frac{K_B T_{peak}}{hA}\right) \tag{2.8}$$

$$\Delta S = \frac{\Delta H - T\Delta G}{T_{peak}} \tag{2.9}$$

In this case, K_B stands for the Boltzmann constant, h for the Planck constant, and T_{peak} for the maximal decomposition temperature from the DTG peak.

3. RESULTS and DISCUSSION

In this part, the results of the preliminary characterization of *C. vulgaris*, including proximate and elemental analyses, are first presented. Then, the results obtained from TGA combined with MS and FTIR are discussed in detail. We used different kinetic models to find the activation energies and thermodynamic parameters that occur along with the pyrolysis process. Simultaneous FTIR and MS spectra were used to analyze the gaseous species that came out during thermal decomposition in real time. The result helped us figure out how the breakdown happened. After that, the findings of the pyrolysis tests in a fixed-bed reactor are discussed. The Box-Behnken method was used to design the experiment, and the findings are shown in both graphs and tables. Finally, the solid and liquid products obtained under optimum pyrolysis conditions were thoroughly characterized.

3.1. The characteristics of the *Chlorella vulgaris*

Table 3.1 illustrates that *C. vulgaris* had 5.55 wt.% moisture and 75.80 wt.% volatile matter, which made up the total biomass. The ash content of *C. vulgaris* was 7.81 wt.%, and the fixed carbon content was 10.84 wt.%, which was found by calculating 100% and subtracting the percentages of moisture, volatile, and ash. An ultimate analysis was done to find out what elements were in the microalgae biomass in addition to the proximate analysis. The average elemental contents (wt.%) were as follows: carbon ($48.62 \pm 0.40\%$), hydrogen ($6.75 \pm 0.09\%$), nitrogen ($8.24 \pm 0.17\%$), and sulfur ($1.03 \pm 0.08\%$). The amount of oxygen was found to be 35.36 ± 0.10 wt.%.

The Dulong formula was used to determine the higher heating value (HHV) of *C. vulgaris* based on its elemental composition. The HHV, which was calculated, was 19.90 MJ/kg, which means it has a moderate amount of energy. This value was in line with the reported values for *C. vulgaris*, which had HHVs of 19.3 MJ/kg [63], 21.25 MJ/kg [64], and 22.19 MJ/kg [65], as well as *Chlorella* sp. KR1, which had a reported value of 24.61 MJ/kg [66].

Table 3.1. Results of the proximate and ultimate analysis.

Proximate analysis	***C. vulgaris***	***Biochar***
Moisture	5.55	4.12
Volatiles	75.80	13.06
Ash	7.81	9.77
Fixed C*	10.84	73.05
Ultimate analysis		
C	48.62 ± 0.40	80.76 ± 0.95
H	6.75 ± 0.09	3.52 ± 0.84
S	1.03 ± 0.08	1.09 ± 0.27
O	35.36 ± 0.10	4.69 ± 0.27
H/C	1.65	0.52
O/C	0.55	0.04
Calorific value (MJ/kg)	**19.90**	**31.59**

After pyrolysis, the obtained biochar showed significant variations in its composition, which shows that the thermal transformation was successful. The biochar had a lot more fixed carbon (73.05 wt.%), as well as 13.06 wt.% volatile matter, 9.77 wt.% ash, and 4.12 wt.% moisture. Elemental analysis showed that the carbon level increased (80.76 ± 0.95%) and the hydrogen, sulfur, and oxygen levels decreased (3.52 ± 0.84%, 1.09 ± 0.27%, and 4.69 ± 0.27%, respectively). These changes show that the biomass was more carbonized and structurally aromatized during pyrolysis. The HHV of the biochar was found to be 31.59 MJ/kg, which is a significant increase from the raw microalgae and shows that energy densification works well.

3.2. Morphological characterization

Figure 3.1a displays untreated SEM images of *C. vulgaris*. The surface is smooth. Table 3.2 shows that the BET analysis shows a low specific surface area of 4.62 ± 0.20 m^2/g. EDS and elemental mapping (Figure 3.2) show that most of the biomass is made up of carbon (C) and oxygen (O). There are low levels of sodium, calcium, magnesium, potassium, and sulfur. Pyrolysis makes a big difference in biochar

(Figure 3.1b). The SEM image shows a surface that is porous and fragmented, which shows how internal volatiles change and how cellular structures break down when they are heated. The BET surface area additionally increases substantially, to 161.26 ± 0.80 m^2/g, which means that a lot of pores have formed. Table 3.3 shows the detailed adsorption data that were used to determine the BET surface area. The EDS spectra of the biochar show that it has more carbon, hydrogen (H), and higher levels of Ca, Mg, and K. These elements are likely to present as thermally stable mineral residues, like oxides or carbonates (Figure 3.3). The biochar has more pores and minerals than the raw biomass, which are important for making it a better synthetic energy material.

3.3. Structural characterization

Figure 3.4 shows the XRD patterns of *C. vulgaris* before and after pyrolysis. The raw biomass shows a wide, low-intensity diffraction peak at $2\theta \approx 20.0°$, which is a sign of an amorphous structure that is common in organic biomolecules like proteins, lipids, and carbohydrates [42]. After pyrolysis, the biochar's XRD pattern showed a significant modification in structure. At about $2\theta \approx 26.0°$, a sharper and more intense peak appeared. This peak corresponded to the (002) plane of graphitic carbon, which means that some graphitization had taken place and turbostratic carbon structures had formed. This means that heating carbon up makes it more likely to aromatize and rearrange itself into more ordered domains. There is a smaller peak at $2\theta = 43.0°$ that is linked to the (100) plane of hexagonal graphite. This supports the idea that graphitic microcrystallites are making microcrystallites [43]. The existence of additional minor peaks between $2\theta = 20°$ and 40° may indicate the formation or enhancement of inorganic crystalline phases during pyrolysis.

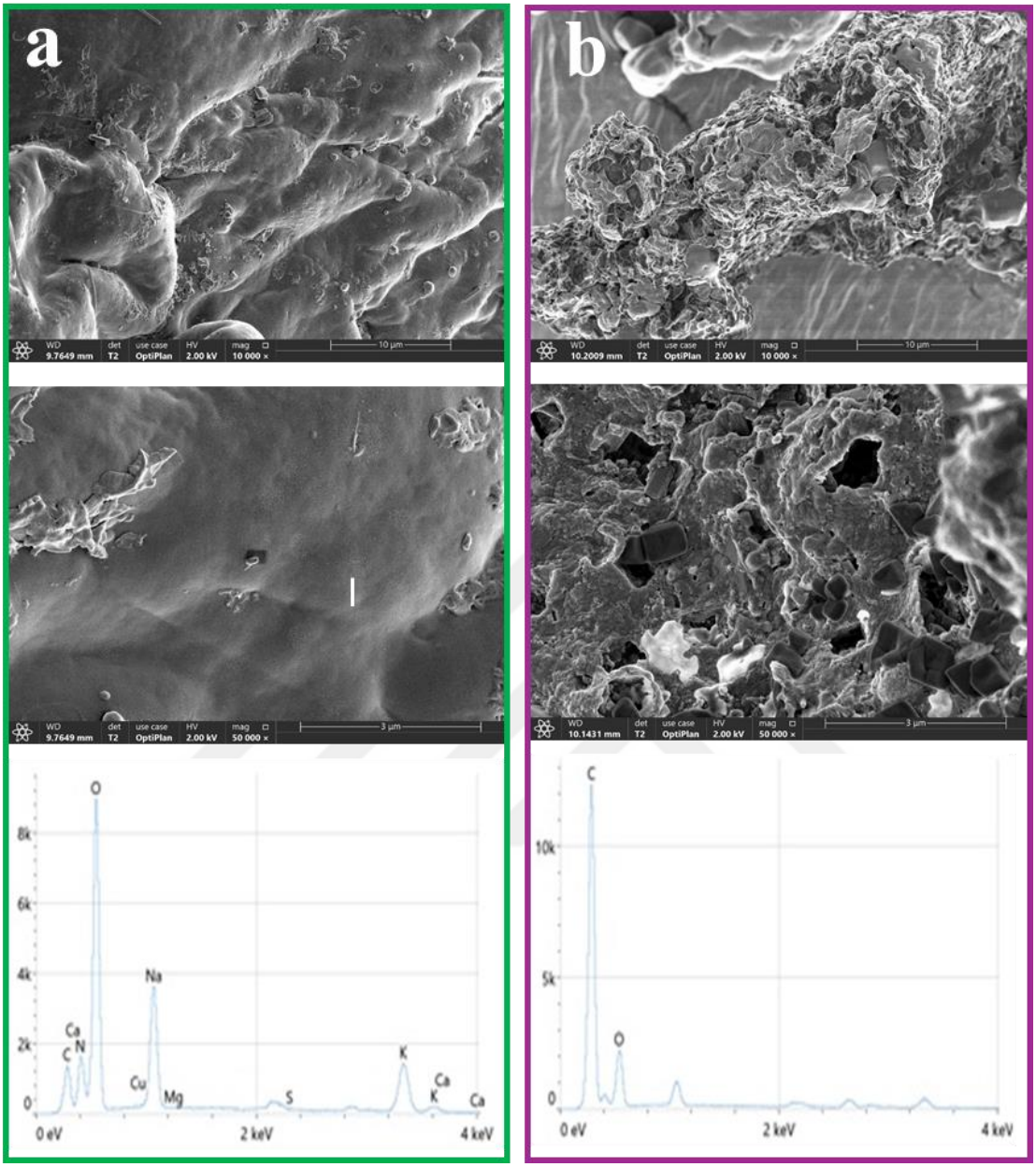

Figure 3.1. SEM image and corresponding EDS spectrum of (a) raw *Chlorella vulgaris*, and (b) biochar obtained after pyrolysis at different magnification levels.

Table 3.2. Nitrogen adsorption data and BET surface area parameters for raw *Chlorella vulgaris* determined at 77 K using the BET method.

Relative Pressure (p/p^0)	Quantity Adsorbed (cm^3/g STP)	$1/[Q(p^0/p - 1)]$ (g/cm^3 STP)
0.0575	0.4623	0.132058
0.0599	0.5450	0.117040
0.0918	0.6367	0.158839
0.1000	0.6917	0.160680
0.1250	0.7726	0.185011
0.1501	0.8556	0.206459
0.1749	0.9480	0.223715
0.2000	1.0034	0.249159

Table 3.3. Nitrogen adsorption data and BET surface area parameters for biochar derived from Chlorella vulgaris, measured at 77 K using the BET method.

Relative Pressure (p/p^0)	Quantity Adsorbed (cm^3/g STP)	$1/[Q(p^0/p - 1)]$ (g/cm^3 STP)
0.0539	34.9184	0.001633
0.0740	36.8350	0.002170
0.1019	39.0008	0.002887
0.1269	40.8327	0.003560
0.1526	42.5537	0.004286
0.1778	44.1778	0.004896
0.2030	45.7784	0.005578
0.2292	47.4022	0.006274
0.2546	49.0750	0.006984
0.2803	50.6003	0.007665
0.3059	52.2480	0.008438

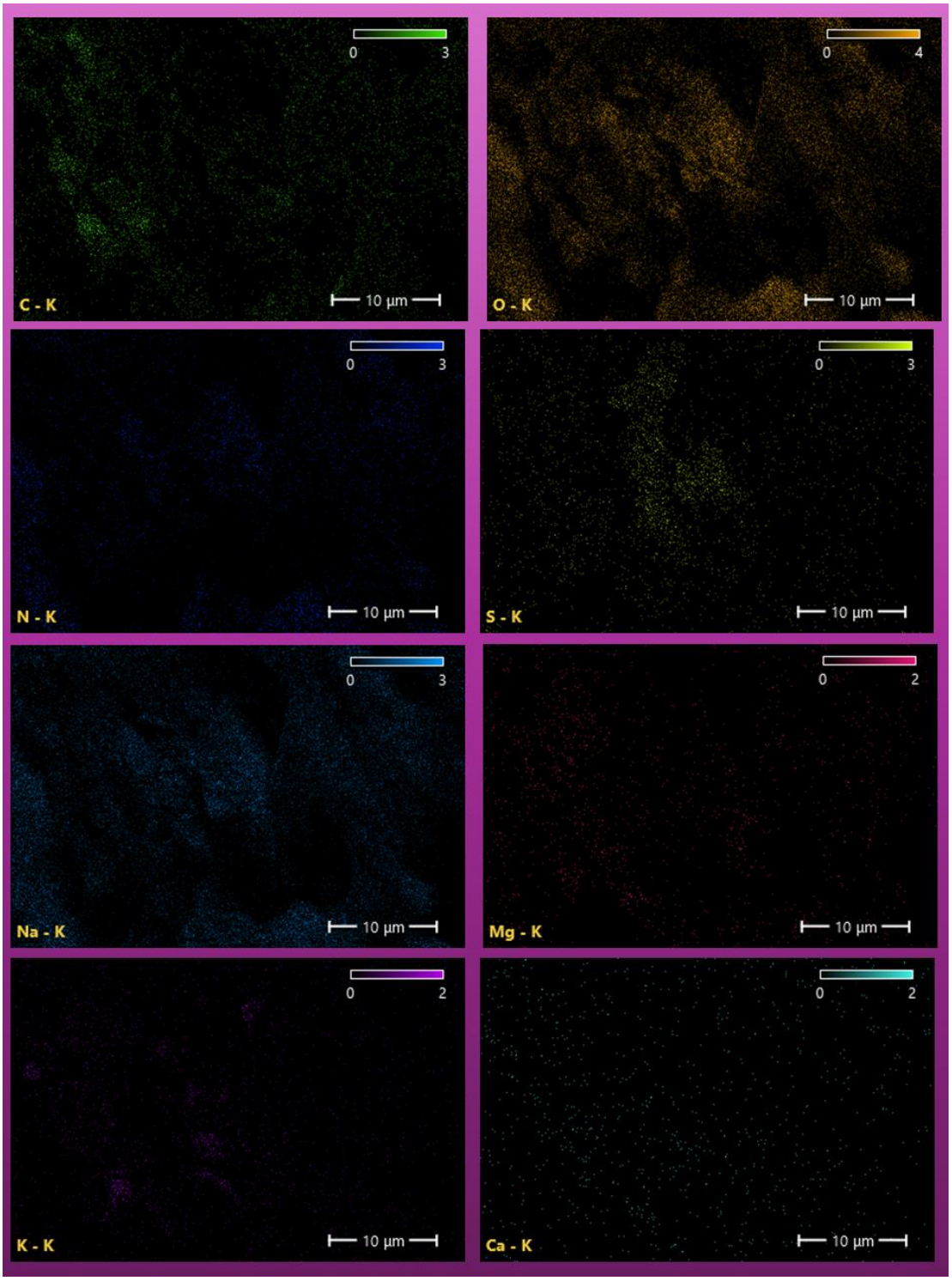

Figure 3.2. FE-SEM elemental mapping images of raw *Chlorella vulgaris*.

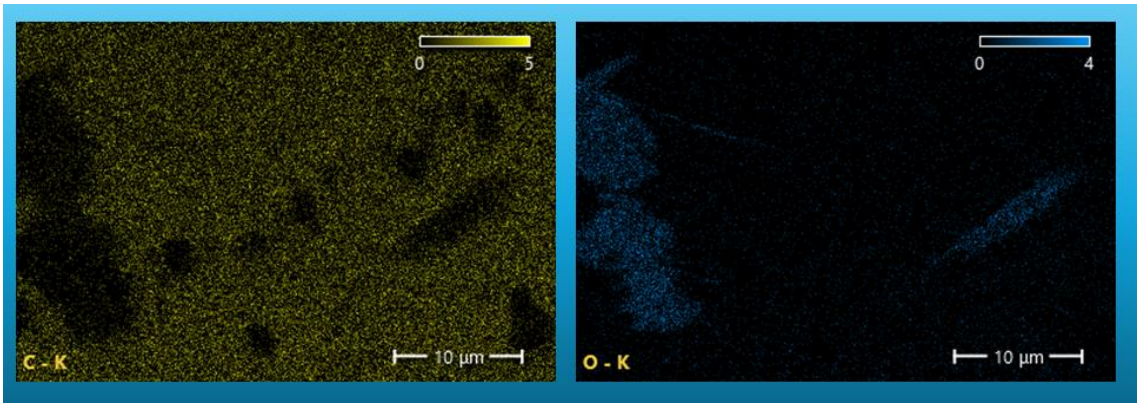

Figure 3.3. FE-SEM elemental mapping images of *Chlorella vulgaris*-derived biochar after pyrolysis.

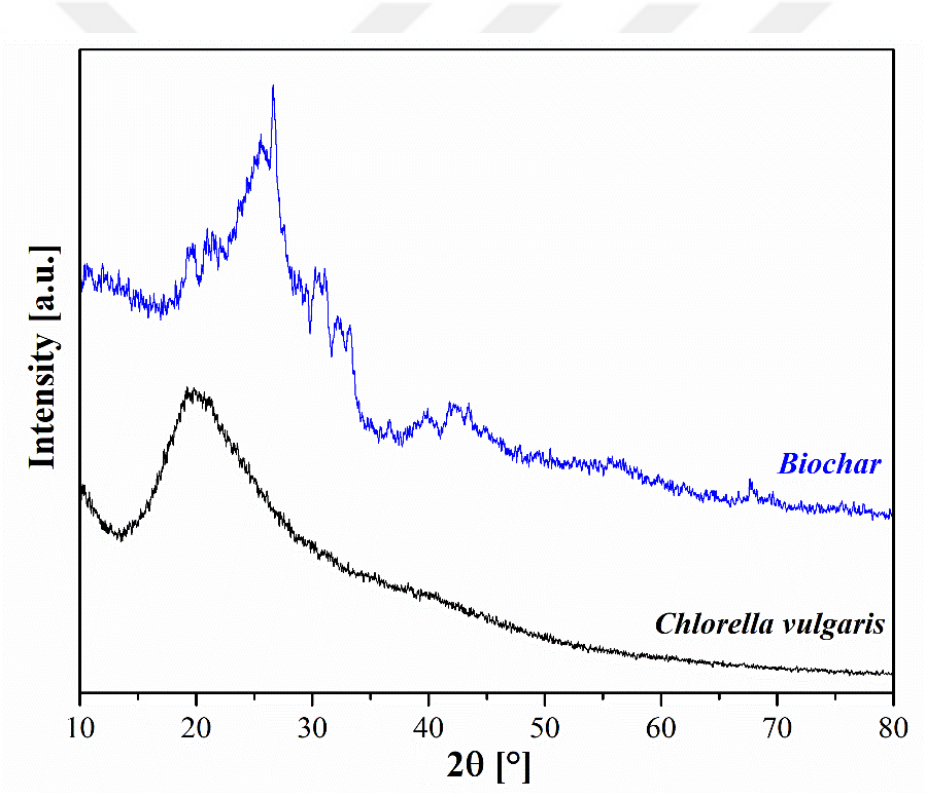

Figure 3.4. X-ray diffraction (XRD) patterns of *Chlorella vulgaris* before and after pyrolysis.

The SEM-EDS study results also back this theory by showing that there were Ca, Mg, and K, which might have been carbonates or oxides. In short, the XRD measurements show that the pyrolyzed biochar has some crystalline graphitic structures. This proves that it has changed from an amorphous biopolymeric matrix to a more ordered carbonaceous material. This shows that it can be used as a solid fuel and also shows how useful it is to make two useful products: bio-oil as a liquid fuel and biochar as a solid fuel. This method helps get more energy back and makes the pyrolysis process work better.

Along with the XRD results, FTIR analysis was used to gain insight into the chemical properties of *C. vulgaris* before and after pyrolysis (Figure 3.5). The FTIR spectrum of the untreated microalgae shows a wide absorption band around 3400 cm^{-1}, This band corresponds to O–H and N–H stretching vibrations, which means that hydroxyl and amide functional groups are present. These groups mostly come from proteins and polysaccharides. There is a distinct band near 2920 cm^{-1} that matches C–H stretching in aliphatic chains. This is usually associated with lipids and carbohydrates. Strong absorption peaks at ~1650 cm^{-1} (amide I) and ~1540 cm^{-1} (amide II) are assigned to C=O stretching and N–H bending, confirming the presence of proteinaceous structures. Additional bands between 1000–1200 cm^{-1} are linked to C–O and C–O–C stretching vibrations, characteristic of polysaccharides [44–46].

Following pyrolysis, these functional groups are largely diminished or disappear, particularly the O–H, N–H, and C–H bands, indicating the decomposition of thermally labile biomolecules and the loss of hydrogen- and oxygen-containing functionalities. The resulting biochar spectrum is dominated by signals associated with aromatic and condensed structures, confirming the formation of a more thermally stable, carbon-rich matrix in line with the carbonization process.

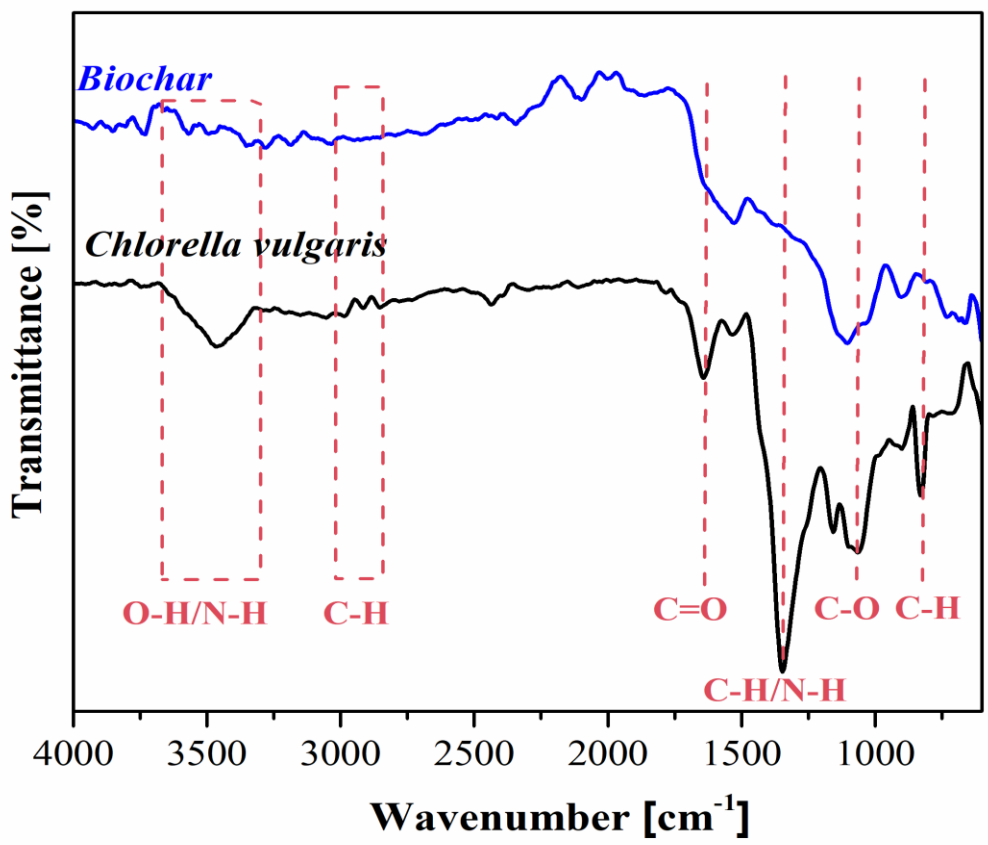

Figure 3.5. Fourier-transform infrared (FTIR) spectra of *Chlorella vulgaris* before and after pyrolysis.

3.4. Thermal decomposition behavior of *Chlorella vulgaris*

The thermal degradation behavior of *C. vulgaris* was investigated using TGA and derivative thermogravimetric (DTG) analysis at three different heating rates under a nitrogen atmosphere. The corresponding TGA and DTGA profiles are presented in Figures 3.6a–3.6b, while the characteristic decomposition temperatures are summarized in Table 3.4.

Table 3.4. Thermal decomposition characteristics of *Chlorella vulgaris* at the active pyrolysis region.

β (°C/min)	T_i (°C)	T_{peak} (°C)	T_f (°C)
10	156.4	305.2	521.1
20	170.2	319.9	561.0
30	192.1	342.2	582.2

The TGA curves of *C. vulgaris* exhibited a typical three-stage weight-loss profile, consistent with that of previous studies on microalgal pyrolysis [3,47]. The first step of mass loss started at around 150 °C and was caused by the evaporation of moisture that was physically adsorbed. This area was rather stable, no matter how fast the heating was performed. This suggests that the moisture was weakly bound and not substantially affected by changes in heating rate. The second step, which was the active pyrolysis zone, took place between 150 and 585 °C. Because heat breaks down and releases volatile substances from biological macromolecules, this region lost the most weight [48]. Peak intensity increases with heating rate. The T_{peak} value was 305.2 °C at 10 °C/min and 342.2 °C at 30 °C/min. These changes occur faster when the heating rate is higher because of thermal lag effects and less effective heat transfer. The DTG curves also showed that the peaks got sharper and the rate of weight loss increased as the temperature rose. This means that when the temperature rises, thermal decomposition happens faster. The TG and DTG curves didn't vary much in shape, but they did change in how they reacted to heat. To put it another way, increasing the rate at which the material heats up doesn't change how it breaks down.

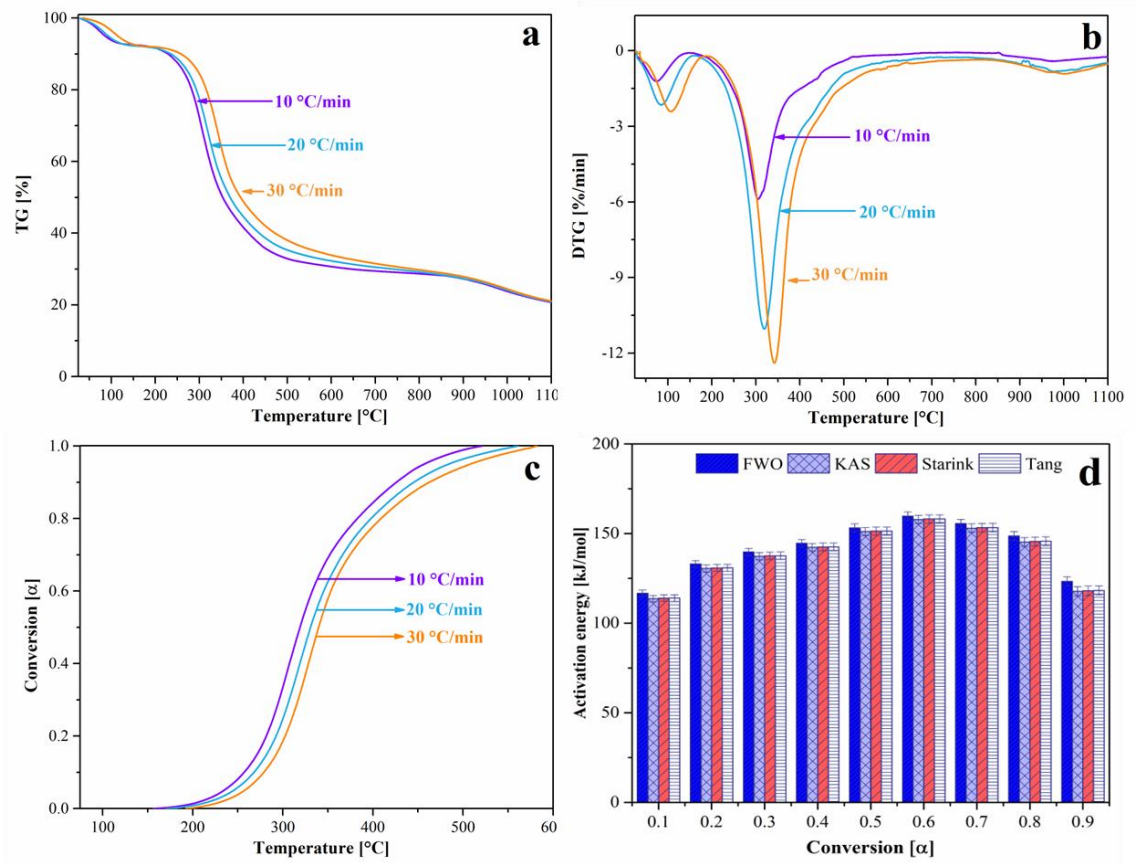

Figure 3.6. (a) TGA and (b) DTG curves; (c) conversion versus temperature profiles at different heating rates; (d) changes in activation energy (E, kJ/mol) in connection with the degree of conversion during the thermal decomposition of *Chlorella vulgaris*.

The third stage, which began about 600 °C, exhibited a gradual and slight decrease in mass attributed to the carbonization of residual biomass. At this time, cross-linked aromatic structures, thermally stable macromolecules, and minerals (such as alkali/alkaline earth metals that produce ash) probably all had a part in the slow breakdown and formation of solid char. The second stage had a stronger passive pyrolysis zone; however, this one was highly crucial for the final product of biochar synthesis. The experimental data indicate that the heating rate substantially influences the thermal decomposition characteristics and kinetics of *C. vulgaris*. The observed variation in degradation temperatures and peak intensities highlights the significance of thermal transfer and reaction rate coupling in non-isothermal pyrolysis processes.

3.5. Kinetics and thermodynamic assessment of *Chlorella vulgaris*

We need to learn more about the kinetics and thermodynamics of pyrolysis to increase the efficiency of the thermal analysis process. Therefore, model-free iso-conversional techniques—Flynn–Wall–Ozawa (FWO), Kissinger–Akahira–Sunose (KAS), Starink, and Tang—were used to investigate the decomposition of *C. vulgaris* over a conversion interval of α = 0.1 to 0.9. The obtained activation energies and thermodynamic parameters are compiled in Tables 3.5, 3.6, and 3.7. In addition, the variation of *ΔH*, *ΔG*, and *ΔS* values with conversion at different heating rates, as determined by the FWO, KAS, Starink, and Tang models, is presented in Figures 3.7–3.10. Figure 3.6c illustrates the relationship between conversion and temperature at various heating rates, while the dependence of E on the extent of conversion is shown in Figure 3.6d.

Table 3.5. Activation energies (E, kJ/mol) with respect to conversion degrees for pyrolysis of *Chlorella vulgaris*.

Conversion	**FWO**		**KAS**		**Starink**		**Tang**	
α	**E**	**R^2**	**E**	**R^2**	**E**	**R^2**	**E**	**R^2**
0.1	116.6	0.9799	113.7	0.9766	113.9	0.9767	114.0	0.9768
0.2	133.0	0.9855	130.5	0.9833	130.8	0.9833	130.8	0.9834
0.3	139.6	0.9891	137.3	0.9875	137.5	0.9875	137.6	0.9876
0.4	144.5	0.9934	142.2	0.9924	142.5	0.9924	142.5	0.9924
0.5	153.1	0.9957	151.1	0.9950	151.3	0.9951	151.4	0.9951
0.6	159.7	0.9999	157.8	0.9999	158.1	0.9999	158.1	0.9999
0.7	155.5	0.9998	153.0	0.9988	153.3	0.9998	153.3	0.9998
0.8	148.5	0.9975	145.3	0.9970	145.6	0.9971	145.6	0.9971
0.9	123.3	0.9897	117.7	0.9874	118.1	0.9875	118.2	0.9876
Average	**141.5±3.72**		**138.7±3.94**		**139.0±4.05**		**139.1±3.39**	

Table 3.6. Thermodynamic parameters at 20 °C/min using FWO and KAS models.

	FWO				KAS			
α	**A**	**ΔH**	**ΔG**	**ΔS**	**A**	**ΔH**	**ΔG**	**ΔS**
0.1	1.48×10^{10}	111.7	149.8	-64.2	7.96×10^{9}	108.7	149.9	-69.4
0.2	4.68×10^{11}	128.1	149.1	-35.5	2.78×10^{11}	125.6	149.2	-39.9
0.3	1.89×10^{12}	134.7	148.9	-23.9	1.15×10^{12}	132.3	149.0	-28.1
0.4	5.30×10^{12}	139.6	148.7	-15.4	3.26×10^{12}	137.3	148.8	-19.4
0.5	3.19×10^{13}	148.2	148.4	-0.4	2.08×10^{12}	146.1	148.5	-4.0
0.6	1.27×10^{14}	154.8	148.2	11.1	8.49×10^{13}	152.9	148.3	7.7
0.7	5.22×10^{13}	150.5	148.4	3.7	3.10×10^{13}	148.0	148.4	-0.7
0.8	1.25×10^{13}	143.7	148.6	-8.2	6.15×10^{12}	140.3	148.7	-14.1
0.9	6.02×10^{10}	118.3	149.5	-52.6	1.88×10^{10}	112.8	149.7	-62.2
Av.	2.57×10^{13}	136.6	148.8	-20.6	1.64×10^{13}	133.8	148.9	-25.6

Table 3.7. Thermodynamic parameters at 20 °C/using Starink and Tang models.

α	Starink				Tang			
	A	**ΔH**	**ΔG**	**ΔS**	**A**	**ΔH**	**ΔG**	**ΔS**
0.1	8.42×10^{9}	109.0	149.9	-68.9	8.49×10^{9}	109.0	149.9	-68.9
0.2	2.94×10^{11}	125.9	149.2	-39.4	2.96×10^{11}	125.9	149.2	-39.3
0.3	1.22×10^{12}	132.6	149.0	-27.6	1.23×10^{12}	132.6	149.0	-27.5
0.4	3.46×10^{12}	137.6	148.8	-18.9	3.47×10^{12}	137.6	148.8	-18.9
0.5	2.20×10^{13}	146.4	148.5	-3.5	2.21×10^{13}	146.4	148.5	-3.5
0.6	9.01×10^{13}	153.1	148.3	8.2	9.05×10^{13}	153.2	148.3	8.2
0.7	3.30×10^{13}	148.3	148.4	-0.2	3.32×10^{13}	148.4	148.4	-0.1
0.8	6.60×10^{12}	140.7	148.7	-13.5	6.65×10^{12}	140.7	148.7	-13.5
0.9	2.04×10^{10}	113.2	149.7	-61.6	2.07×10^{10}	113.3	149.7	-61.5
Av.	1.74×10^{13}	134.1	148.9	-25.0	1.75×10^{13}	78.3	113.8	-77.6

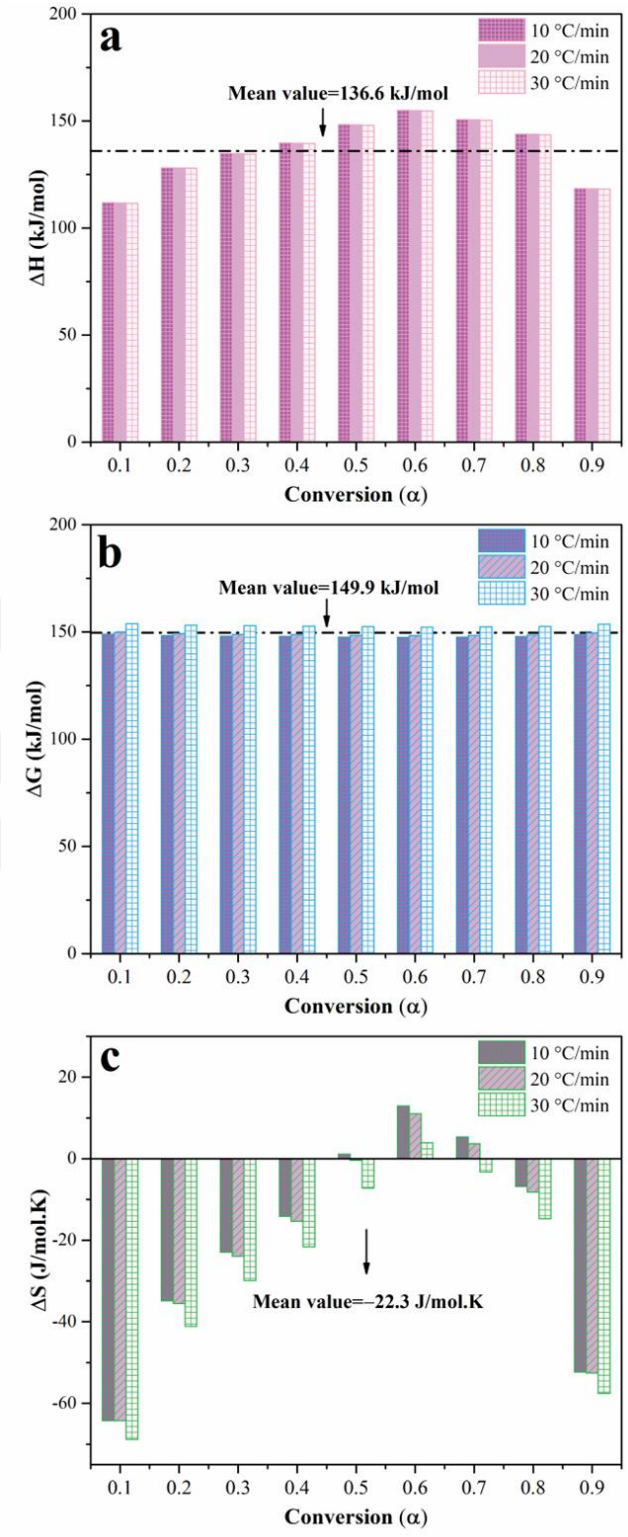

Figure 3.7 (a) Δ*H*, (b) Δ*G*, and (c) Δ*S* values obtained using the FWO model at different heating rates.

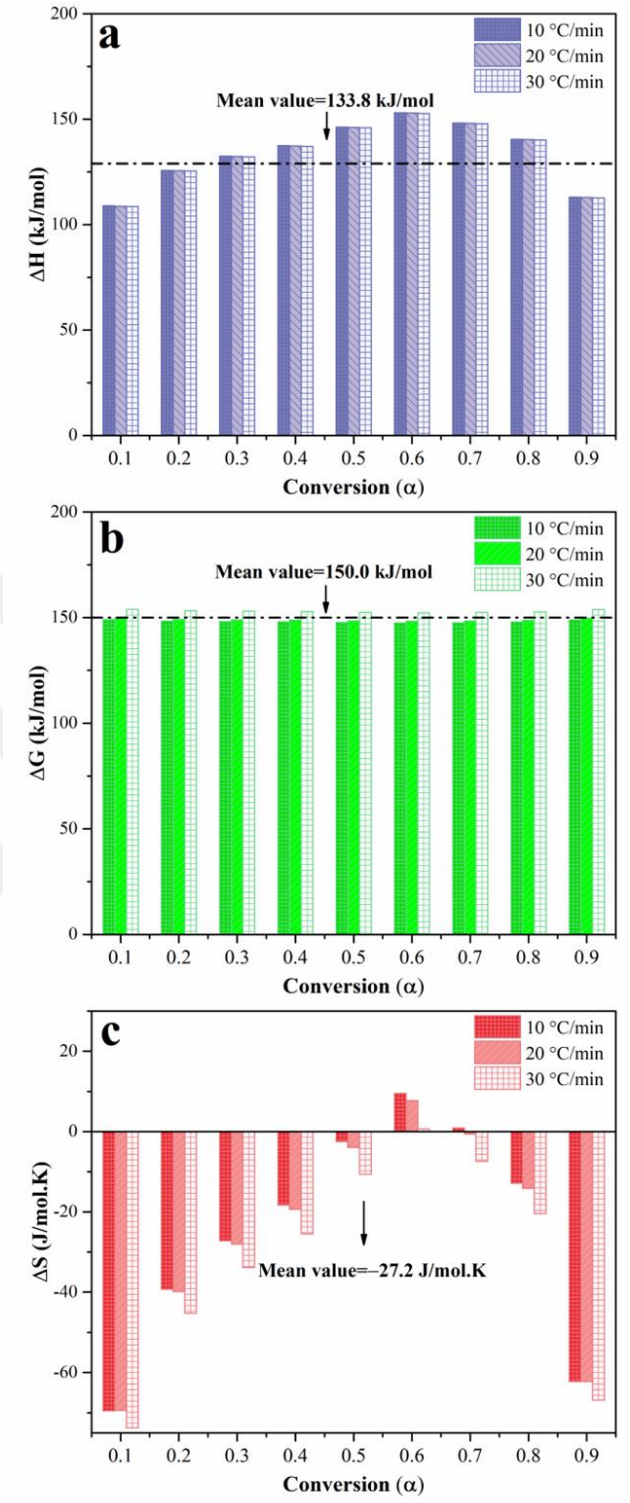

Figure 3.8. a) Δ*H*, b) Δ*G*, and c) Δ*S* values obtained using the KAS model at different heating rates.

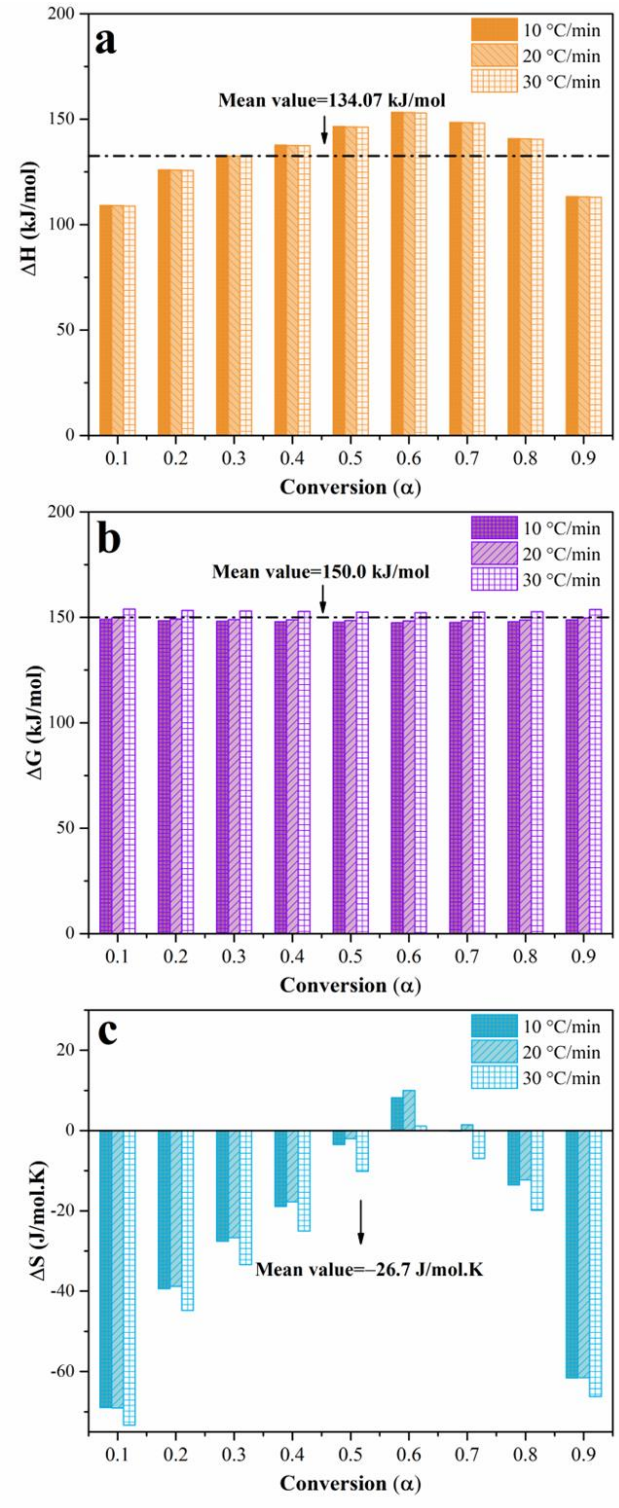

Figure 3.9. a) Δ*H*, b) Δ*G*, and c) Δ*S* values obtained using the Starink model at different heating rates.

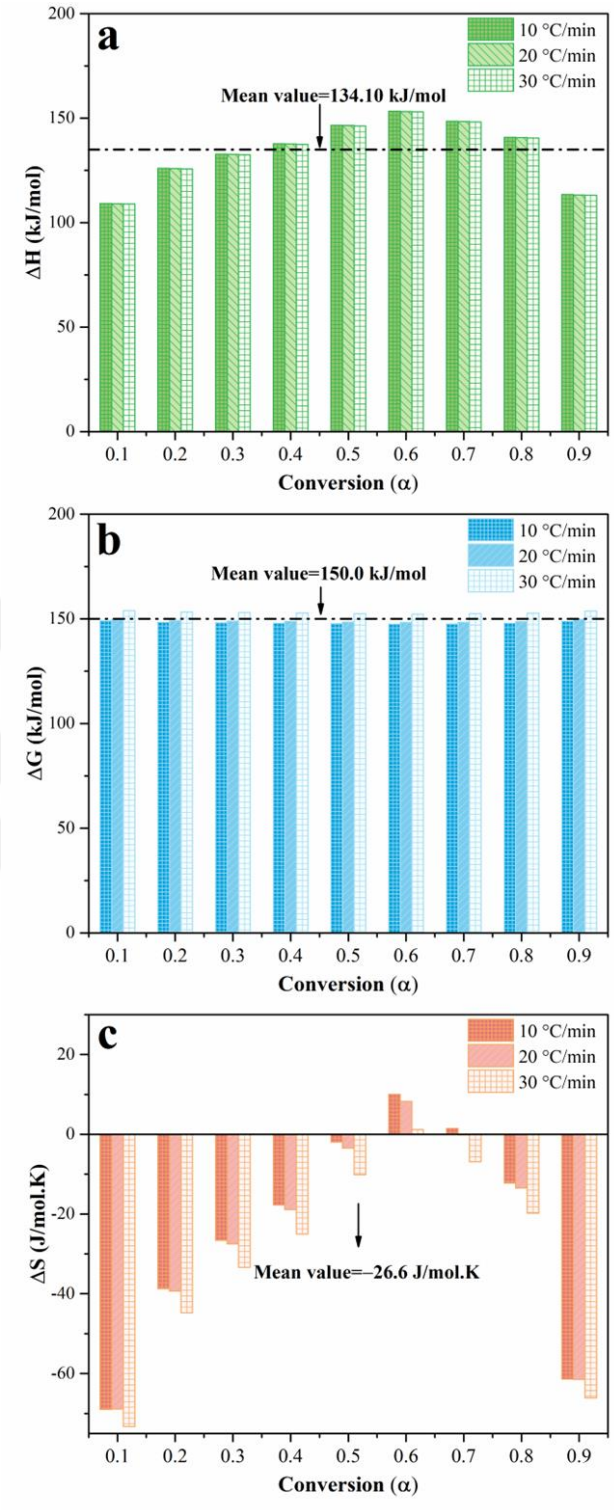

Figure 3.10. a) Δ*H*, b) Δ*G*, and c) Δ*S* values obtained using the Tang model at different heating rates.

Linear iso-conversional plots for each method (Figs. 3.11a-d) exhibited high correlation coefficients ($R^2 \geq 0.9766$), confirming the robustness and applicability of the selected models in describing the pyrolytic behavior of *C. vulgaris*. The linearity observed in the plots of ln(β), ln(β/T), ln(β/$T^{1.92}$), and ln(β/$T^{1.8947}$) versus 1/T across all α values supports the reliability of the iso-conversional approach.

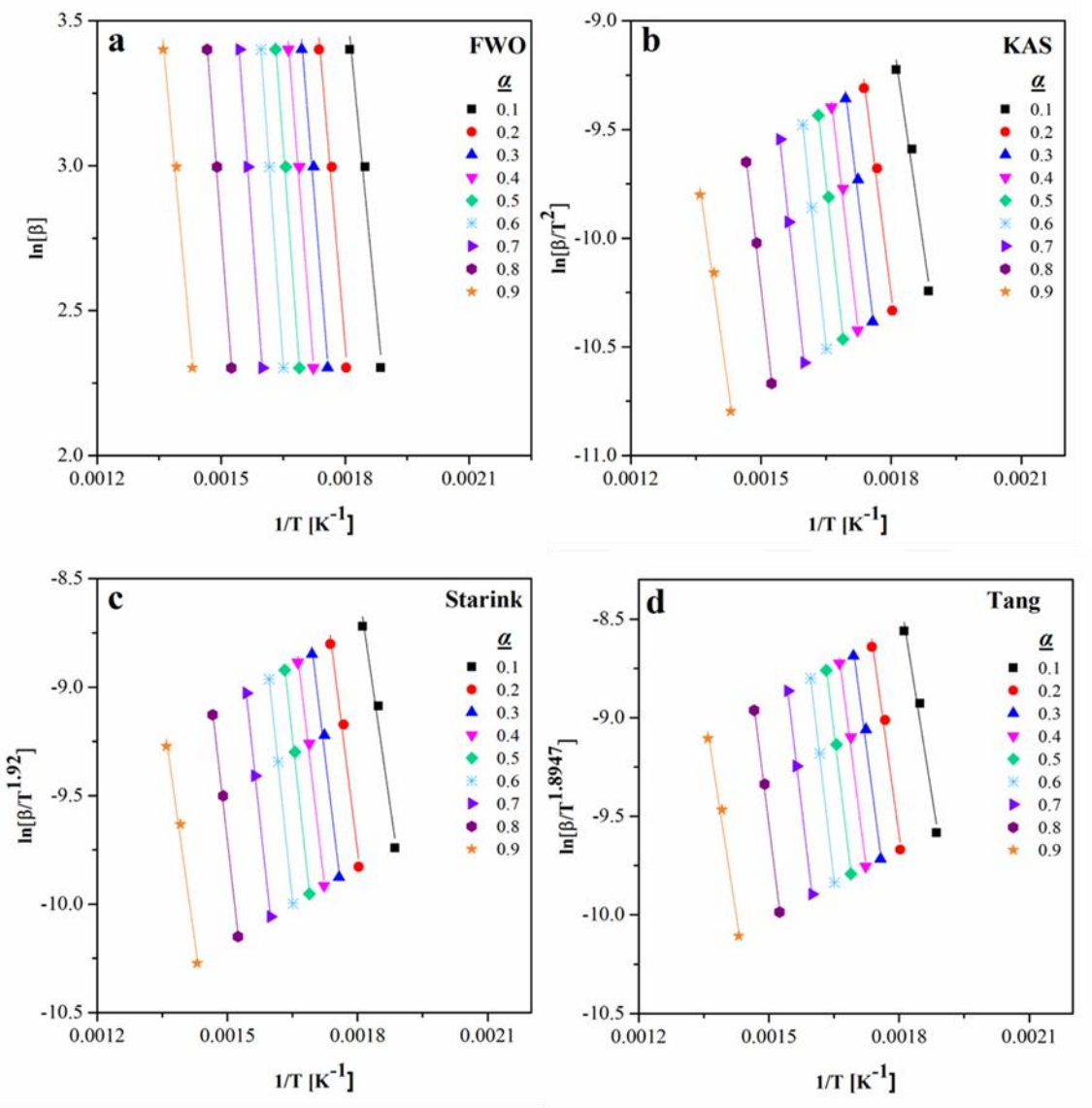

Figure 3.11. Isoconversional plots for the pyrolysis of *Chlorella vulgaris* obtained using different model-free methods: (a) Flynn–Wall–Ozawa (FWO), (b) Kissinger–Akahira–Sunose (KAS), (c) Starink, and (d) Tang methods, at various conversion levels (α = 0.1–0.9).

The activation energy exhibited an increasing trend from α = 0.1 to 0.6, reflecting the progressive breakdown of structurally stable biomolecules such as proteins and lipids. At higher conversion levels (α = 0.8–0.9), a slight decline in E was observed. The activation energies from the FWO, KAS, Starink, and Tang techniques were all very similar: 141.5, 138.7, 139.0, and 139.1 kJ/mol. This illustrates that the procedures are all very similar, and these values align well with those reported in the literature. For example, in the non-catalytic pyrolysis of *Chlorella* species, average activation energies of 156.16 kJ/mol (KAS), 158.10 kJ/mol (FWO), 156.44 kJ/mol (Starink), and 156.53 kJ/mol (Vyazovkin) have been reported [49]. Other studies applying the KAS method have also reported activation energies ranging from 97.22 to 335.69 kJ/mol, depending on biomass characteristics and pyrolysis conditions [50–52]. Similarly, values such as 298.42 kJ/mol (FWO) and 301.70 kJ/mol (KAS) were obtained for extracted *Chlorella* biomass [53]. The results of the present study fall within the broad range reported in the literature, further confirming the reliability and applicability of the model-free iso-conversional methods for analyzing the pyrolysis kinetics of *C. vulgaris*.

3.6. TGA/FTIR/MS analysis of *Chlorella vulgaris*

The evolution of gaseous products during *C. vulgaris* thermal decomposition was investigated using TGA–FTIR at 20 °C/min heating rate under nitrogen. The data are presented as Gram-Schmidt signals, 3D FTIR spectra, and absorbance versus time profiles for selected functional groups (Figure 3.12).

The Gram-Schmidt curve (Fig. 3.12a), which reflects the total infrared absorbance over time, indicates the global evolution of volatile compounds. A major peak is observed at approximately 350 °C, indicating the main devolatilization phase, which corresponds to the primary weight loss step in the TGA data. Additionally, a secondary shoulder at around 950 °C indicates a possible late-stage release of minor volatiles. The 3D FTIR spectrum is given in Fig. 3.12b. Key absorption peaks detected in regions corresponding to CO_2 (2351 cm^{-1}), CO (2171 cm^{-1}). These processes are typically associated with the thermal breakdown of carboxylic, carbonyl, and hydroxyl-containing components, such as proteins, carbohydrates, and lipids inherent in algal biomass [54].

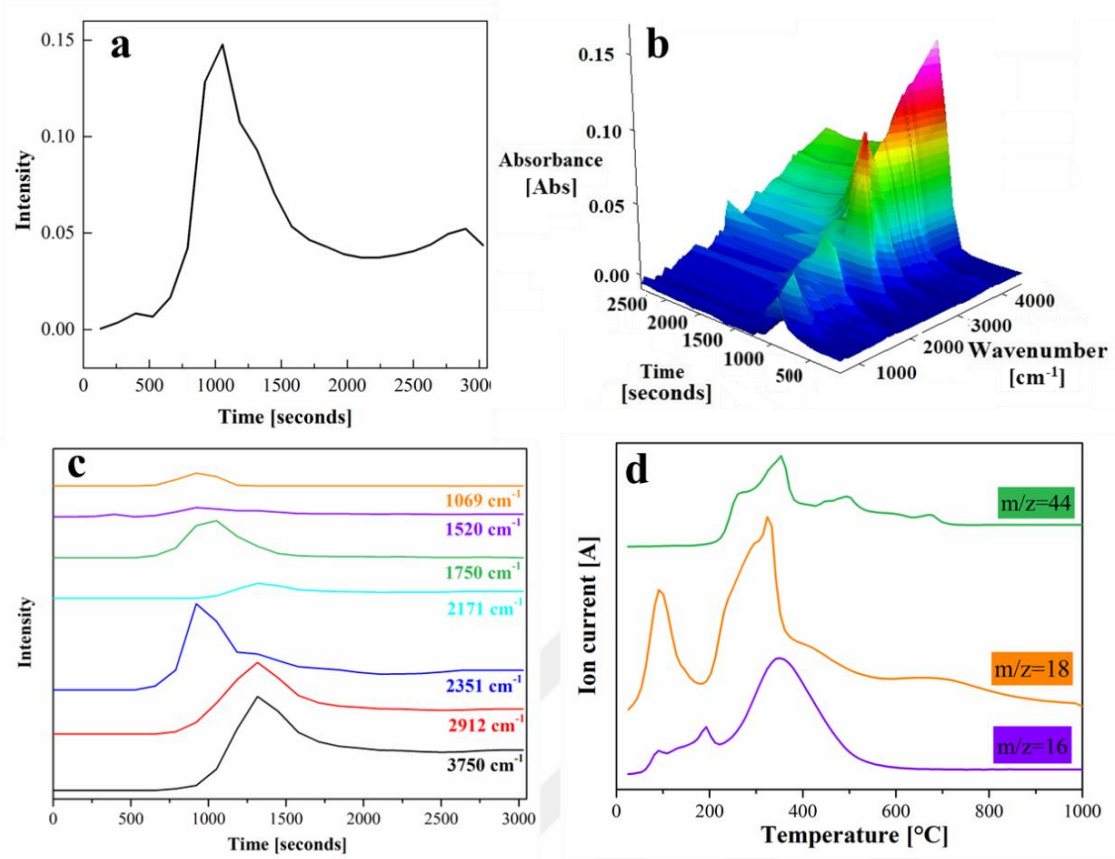

Figure 3.12. (a) Gram–Schmidt curve; (b) three-dimensional (3D) FTIR spectrum; (c) selected absorbance intensities at characteristic wavenumbers over time for volatile species evolved from *Chlorella vulgaris*; (d) single ion current curves (m/z = 16, 18, and 44) for major gaseous products detected during the pyrolysis of *Chlorella vulgaris.*

To show how gases evolve, absorbance intensities at certain wavenumbers were displayed with time (Fig. 3.12c). The CO_2 peak, which is around 2351 cm^{-1}, reaches its highest point around 350 °C, which is the main devolatilization step. At 2171 cm^{-1}, CO shows a similar pattern but with less intensity, which means it is evolving together with CO_2. The 1745 cm^{-1} band is caused by C=O stretching vibrations in aldehydes and ketones. A band at the same temperature suggests lipid structural breakdown. The C=C stretching vibration absorbance near 1520 cm^{-1} shows unsaturated and aromatic species forming conjugated or aromatic compounds. The 2912 cm^{-1} and 3750 cm^{-1} peaks are aliphatic C–H and hydroxyl O–H stretching vibrations. Moisture release or hydroxyl-rich carbohydrate and protein degradation may accelerate O–H band formation.

The 1069 cm^{-1} band shows C–O stretching. Pyrolysis disperses oxygenated alcohols, ethers, and esters [54,55]. These data reveal that *C. vulgaris* degradation is multi-step and produces various gaseous byproducts. The presence of CO_2, CO, water, and oxygenated organic molecules emphasizes the significance of decarboxylation and deoxygenation reactions. Proteins, lipids, and carbohydrates experience simultaneous thermal variations according to infrared band timing and intensity.

To validate FTIR findings and find *C. vulgaris* breakdown gases, we employed TGA–MS under the same heating settings. For varied mass-to-charge ratios (m/z), Figure 3.13d shows ion current intensities as a function of temperature. At 350 °C, the signal at m/z = 44, primarily from CO_2, peaks, aligning with the principal devolatilization phase of the TGA curve. At this temp, decarboxylation is intense. The H_2O ion current at m/z = 18 shows two peaks: one at 150 °C and a larger one around 350 °C. The first peak may represent moisture evaporation and hydroxyl-rich regions releasing water. The second peak may be heat-degrading biomass water. The m/z = 16 signal from CH_4 or O fragments peaks at 350 °C. This suggests glucose and lipid breakdown. These ions' thermal degradation patterns overlap, suggesting microalgal biomass biopolymer breakdown is difficult [3,73,81]. These studies further support the complex decomposition mechanisms involving carbohydrates, proteins, and lipids, and validate the identification of key volatile products across overlapping temperature ranges.

3.7. Py-GC/MS analysis of *Chlorella vulgaris*

In order to study the chemical constituents of pyrolysis products and make gas-phase research better, *C. vulgaris* was quickly pyrolyzed at 500 °C and then analyzed with Py-GC/MS to find out what kinds and amounts of volatile organic chemicals were there. It was found that the pyrolysate was made up of a mix of several chemical substances. We divided these species into basic groups based on the size of their chromatographic regions (Figure 3.13). The pyrolysis products were split into a few main chemical groups, with the following percentages of each group oxygenates (42.6%), nitrogen-containing compounds (25.4%), aromatics (10.8%), aliphatics (alkanes and alkenes combined, 11.9%), phenolics (1.1%), sulfur-containing compounds (0.35%), and other components (3.8%). Aldehydes, ketones, alcohols, acids, ethers, and lactones were all oxygenated substances. This category was the most abundant. The thermal

decomposition of carbohydrates and lipids produces a lot of important compounds, such as n-hexadecanoic acid (13.45%), benzoic acid (7.84%), octadecanoic acid (6.09%), and acetic acid (1.27%). These compounds have a big effect on the chemistry of bio-oil. There were lots of nitrogen-containing compounds, which means that *C. vulgaris* has a lot of protein. Pyrroles, indoles, benzenamine derivatives, and amides were among the identified species. N-hexadecanamide made up 13.60% of the whole thing. Toluene, styrene, ethylbenzene, and p-xylene are examples of aromatic hydrocarbons that make up 10.8% of the pyrolysate. They are useful because there are many methods to use them, and they might be utilized to produce biofuels. Aliphatic hydrocarbons, mostly from lipid cracking and decarboxylation, made up roughly 12% of all the volatile compounds. There were fewer phenolic compounds (1.1%), which are likely generated by breaking down aromatic amino acids and pigments. We found modest amounts of sulfur-containing compounds, principally oxathiane derivatives, that were the same as the quantity of sulfur in the biomass. 3.8% of the pyrolysate is made up of smaller particles. These demonstrate the difficulty in understanding the chemical change occurring during pyrolysis [57,58]. The product's distribution is similar to the chemical makeup of *C. vulgaris*, which implies it could be a good source for making biofuels and biochemicals.

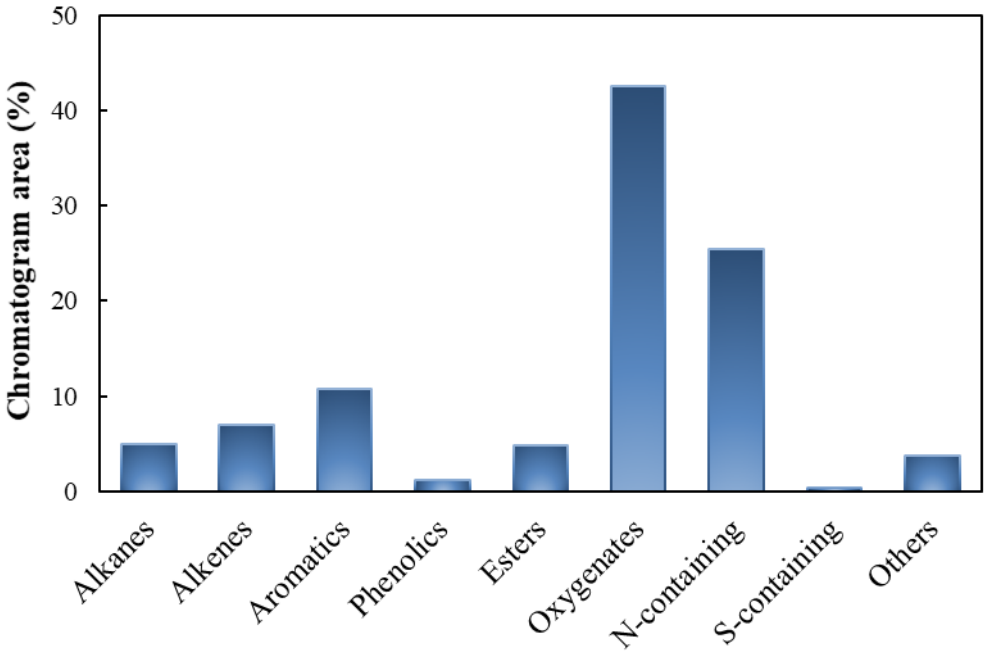

Figure 3.13. Py-GC/MS analysis of volatile product classes obtained from the pyrolysis of *Chlorella vulgaris*.

3.8. Experimental design results

Fixed-bed pyrolysis was enabled by heating the sample at 10 °C/min up to 500 °C under a continuous nitrogen atmosphere with a flow rate of 100 mL/min. Nitrogen was used as an inert carrier gas to minimize secondary reactions during devolatilization and to replicate conditions consistent with the previous thermogravimetric analysis. On a dry ash-free basis, the product distribution consisted of 30.42 wt.% char, 26.10 wt.% bio-oil, and 43.48 wt.% combined gas and water. Because one of the main aims of the present study was to improve bio-oil production, an optimization study was conducted to identify the most favorable pyrolysis parameters. To evaluate how pyrolysis temperature (A), heating rate (B), and nitrogen flow rate (C) jointly affect bio-oil yield from C. vulgaris, BBD was applied. We have performed 15 experiments, and their results are given in Table 3.8.

Table 3.8. Experimental design matrix and corresponding bio-oil yields based on the Box–Behnken design.

Run	**Actual Level of Variables**			**RESPONSE**
Order	Temperature	Heating Rate	Gas Flow Rate	Bio-oil yield (%)
1	500	10	50	25.84
2	500	100	50	32.08
3	500	10	150	26.38
4	500	100	150	32.86
5	400	10	100	17.74
6	400	100	100	25.00
7	600	10	100	22.03
8	600	100	100	28.57
9	400	55	50	22.41
10	400	55	150	24.08
11	600	55	50	24.23
12	600	55	150	28.89
13	500	55	100	29.97
14	500	55	100	28.06
15	500	55	100	28.44

A second-order polynomial model based on coded variables was constructed to represent the correlation between the selected process parameters and the resulting yield. The resulting predictive equation is expressed as follows:

$$\text{Bio-oil yield (\%)} = +28.82 + 1.81A + 3.32B + 0.96C - 0.18AB + 0.75AC + 0.06BC - 4.94A^2 - 0.55B^2 + 1.02C^2$$

This model highlights that the heating rate and temperature positively influenced bio-oil yield, with heating rate exhibiting the strongest effect. The quadratic temperature term (A^2) had a negative coefficient, which meant that the best temperature range was between 500 and 550 °C. We utilized analysis of variance (Table 3.9) to assess the model's validity.

Table 3.9. The results of the analysis of variance (ANOVA) for the quadratic model.

Source	Sum of Squares	df	Mean Square	F-Value	p-value Prob > F
Model	221.40	9	24.60	22.30	0.0016
A-Temperature	26.25	1	26.25	23.79	*0.0046*
B- Heating rate	87.91	1	87.91	79.68	*0.0003*
C-Nitrogen gas flow rate	7.32	1	7.32	6.63	*0.0497*
AB	0.13	1	0.13	0.12	*0.7457*
AC	2.24	1	2.24	2.03	*0.2140*
BC	0.014	1	0.014	0.013	*0.9135*
A^2	90.03	1	90.03	81.59	*0.0003*
B^2	1.12	1	1.12	1.01	*0.3602*
C^2	3.82	1	3.82	3.46	*0.1219*
Residual	5.52	5	1.10	-	-
Lack of Fit	3.47	3	1.16	1.13	0.5006
R^2	0.9757				

The model was important, with an F-value of 22.30. This means that there was only a 0.16% chance that the model fit was due to random noise. The linear terms of temperature, heating rate, nitrogen flow, and the quadratic term of temperature were statistically significant ($p < 0.05$). The modified coefficient of determination (R^2 = 0.9319) and the expected R^2 (0.7349) were very close to each other (less than 0.2), which shows that the model is quite good at making predictions. Additionally, the lack-of-fit test showed no significance ($p > 0.05$), confirming that the model adequately represents the experimental data.

The perturbation plot in Figure 3.14a demonstrates how sensitive the yield of bio-oil is to each process variable while holding the others at their midpoint. The graph reveals that the heating rate has a certain curve, which shows that it is the most essential factor. Temperature and nitrogen flow rate follow next. The yield of bio-oil rose substantially as the heating rate increased, which illustrates how vital it is to the pyrolysis process. Figure 7b indicates that the projected and actual amounts of bio-oil are very similar. The data points are close to line 45, which shows that the model is accurate and reliable. Also, three-dimensional response surface and two-dimensional contour plots (Fig. 3.14) were made to help us see how the process factors interact with each other. Figure 3.14c shows that the amount of bio-oil produced went up with temperature up to around 500 °C, but after that it went down. This was probably because of more secondary cracking and gas generation. There was also a synergistic effect of heating rates, with higher rates helping to make bio-oil. Figure 3.14d shows the combined effect of temperature and nitrogen flow rate. Moderate nitrogen flow rates increased yield, whereas high flow rates and temperatures above 550 °C slowed the synthesis of bio-oil. It could be because the residence durations were shorter, and the rates of volatilization were higher. Figure 7e ultimately shows that the best yields resulted from a high heating rate (80–100 °C/min) and a low nitrogen flow rate (around 100 mL/min).

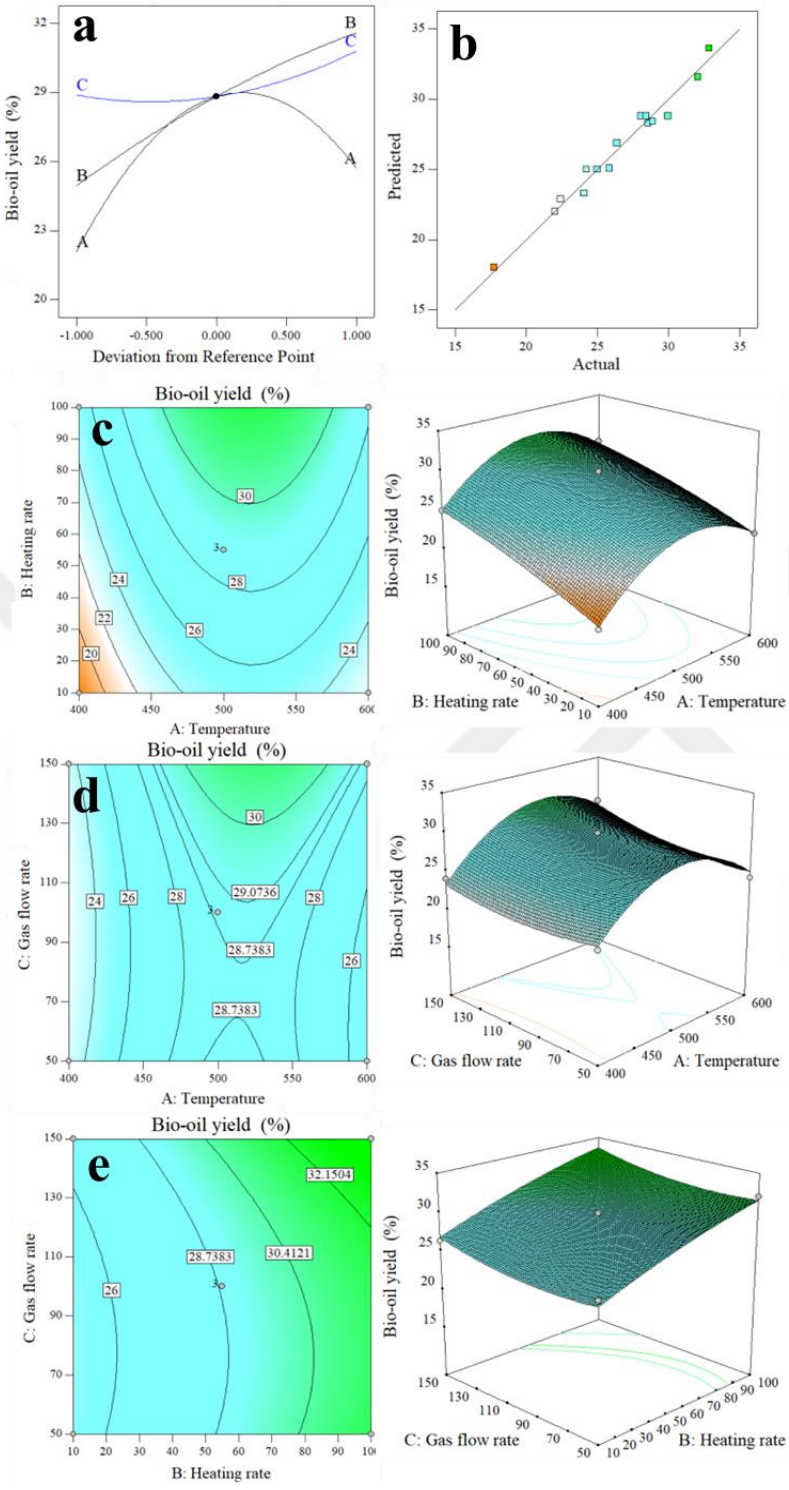

Figure 3.14. (a) Perturbation plots. (b) Predicted vs. actual values of bio-oil yield. (c–e) 3D response surface and contour plots showing the interactions between (c) temperature and heating rate, (d) temperature and nitrogen flow rate, and (e) heating rate and nitrogen flow rate.

3.9. Elemental composition of bio-oil

The bio-oil produced under optimal pyrolysis conditions contained 69.55% carbon, 6.81% hydrogen, 6.24% nitrogen, 1.01% sulfur, and 16.39% oxygen, as indicated by the analysis. The bio-oil has a lot more carbon and a lot less oxygen than raw *C. vulgaris*. This proves that the deoxygenation process worked and that the chemicals now have more energy. The higher heating value (HHV) was 30.40 MJ/kg. The HHV of the raw biomass was 19.90 MJ/kg, which is a substantial increase. This means that the liquid product made by pyrolysis is better fuel. The O to C ratio was 0.28, and the C to H ratio was 1.18. These values show that fuel is less polar and more aromatic than the basic feedstock. This suggests it is more like fossil fuels. This can help the bio-oil stay stable and make it easier to burn. These features are beneficial for fuel because they make the material more stable at high temperatures and provide it with more energy.

4. CONCLUSION

This study thoroughly examined the pyrolysis characteristics of *C. vulgaris* microalgae, highlighting the effects of heating rate, pyrolysis temperature, and nitrogen flow rate on bio-oil yield and composition. The best temperature for generating bio-oil was between 500 and 550 °C, the best heating rate was between 80 and 100 °C/min, and the best nitrogen flow rate was between 100 and 125 mL/min. The kinetic study showed that the pyrolysis process happens through several complicated, multi-step mechanisms. The elemental analysis showed that the amount of carbon increased, and the amount of oxygen decreased. This signifies that the deoxygenation worked and the fuel quality improved. Bio-oil is suitable for thermochemical fuel use since it has a low O/C ratio (0.28) and a high heating value (30.40 MJ/kg). The findings further indicate that *C. vulgaris* bio-oil has chemical characteristics that render it an excellent option for renewable fuel and chemical feedstock applications. The study also emphasized the significance of understanding the interplay between process parameters and biomass quality in enhancing the efficiency of bio-oil production using an experimental design technique. These results improve our understanding of how thermochemical processes can turn micro-algal biomass into valuable chemicals. This could help us find new ways to create bioenergy that is better for the planet.

REFERENCES

[1] A.G. Olabi, M.A. Abdelkareem, Renewable energy and climate change, Renew. Sustain. Energy Rev. 158 (2022) 112111. https://doi.org/10.1016/j.rser.2022.112111.

[2] P. Maciejczyk, L.C. Chen, G. Thurston, The role of fossil fuel combustion metals in PM2.5 air pollution health associations, Atmosphere (Basel). 12 (2021) 1–34. https://doi.org/10.3390/atmos12091086.

[3] I.J.Y. Tan, A.C.M. Loy, B.L.F. Chin, K.W. Cheah, S.Y. Teng, B.S. How, H. Alhazmi, W.D. Leong, H.Y. Lim, M.K. Lam, S.S. Lam, Co-pyrolysis of Chlorella vulgaris with plastic wastes: Thermal degradation, kinetics and Progressive Depth Swarm-Evolution (PDSE) neural network-based optimization, Green Technol. Sustain. 2 (2024) 100077. https://doi.org/10.1016/j.grets.2024.100077.

[4] M.A. Baseer, P. Kumar, E.G.S. Nascimento, Advancements in hydrogen production through the integration of renewable energy sources with AI techniques: A comprehensive literature review, Appl. Energy. 383 (2025) 125354. https://doi.org/10.1016/j.apenergy.2025.125354.

[5] J. Huo, C. Peng, Depletion of natural resources and environmental quality: Prospects of energy use, energy imports, and economic growth hindrances, Resour. Policy. 86 (2023) 104049. https://doi.org/10.1016/j.resourpol.2023.104049.

[6] G.D. Okcu, Microalgae biodiesel production: a solution to increasing energy demands in Turkey, Biofuels. 13 (2022) 77–93. https://doi.org/10.1080/17597269.2019.1637070.

[7] H.E. Jijingi, S.K. Yazdi, Y.A. Abakr, A.D. Maysarah Satya, Exploring the potential of Chlorella vulgaris for nutrient removal and biomass accumulation in palm oil mill effluent (POME): A sustainable and green technology approach, Case Stud. Chem. Environ. Eng. 12 (2025) 101274. https://doi.org/10.1016/j.cscee.2025.101274.

[8] C.H. Lay, V.K. Ponnusamy, K. Trchounian, B. Igliński, G. Piechota, G. Kumar, The renewable energy prospect via pyro-oil blends of Chlorella vulgaris: A Feasibility study, Energy. 334 (2025).

https://doi.org/10.1016/j.energy.2025.137695.

[9] A.R. Mendes, M.P. Spínola, M. Lordelo, J.A.M. Prates, Chemical Compounds, Bioactivities, and Applications of Chlorella vulgaris in Food, Feed and Medicine, Appl. Sci. 14 (2024) 1–26. https://doi.org/10.3390/app142310810.

[10] M.G. Nayak, R.D. Gamit, Parametric study and optimisation of supercritical extraction of Chlorella Vulgaris microalgae using Response surface methodology, Chem. Phys. Impact. 11 (2025) 100923. https://doi.org/10.1016/j.chphi.2025.100923.

[11] L.V. Postolache, G. Soreanu, I. Cretescu, N. Tudorachi, I. Anghel, D.M. Preda, D. Rusu, M.F. Zaltariov, J.L. Valverde, G. Lisa, Alternative energy sources from wastes and microalgae Chlorella vulgaris used for the capture of atmospheric CO2 in the production of cement, Mater. Today Sustain. 31 (2025) 101175. https://doi.org/10.1016/j.mtsust.2025.101175.

[12] J. de Souza Carvalho, W. Artifon, A. da Silva, C.J. de Andrade, D. de Oliveira, Digital transformation of microalgae production: A review of potential optimization strategies for Chlorella vulgaris through intelligent control, Algal Res. 90 (2025). https://doi.org/10.1016/j.algal.2025.104216.

[13] X. Duan, H. Yu, X. Wu, Y. Li, H. Chen, Y. Sun, H. Zheng, B. Wu, A TGA-FTIR study on the pyrolysis of oil-based drilling cuttings and the influence of its solids on pyrolysis characteristics, J. Environ. Chem. Eng. 12 (2024). https://doi.org/10.1016/j.jece.2024.112846.

[14] C.E. Enyoh, P.E. Ovuoraye, M.H. Rabin, W. Qingyue, M.A. Tahir, Thermal degradation evaluation of polyethylene terephthalate microplastics: Insights from kinetics and machine learning algorithms using non-isoconversional TGA data, J. Environ. Chem. Eng. 12 (2024) 111909. https://doi.org/10.1016/j.jece.2024.111909.

[15] Y. Wang, S. Yang, G. Bao, H. Wang, Pyrolytic characteristics of abutilon stalk waste using TG-FTIR, Py-GC/MS, and artificial neural networks: Kinetics, thermodynamics, and gaseous products distribution, J. Anal. Appl. Pyrolysis. 178 (2024) 106403. https://doi.org/10.1016/j.jaap.2024.106403.

[16] M. Altarawneh, Pyrolysis characteristics, thermo-kinetic parameters, and evolved gas analysis for waste biomass derived from food processing industries, Green Technol. Sustain. (2025) 100266. https://doi.org/10.1016/J.GRETS.2025.100266.

[17] B. Mufutau Opeyemi, Path to sustainable energy consumption: The possibility of substituting renewable energy for non-renewable energy, Energy. 228 (2021) 120519. https://doi.org/10.1016/j.energy.2021.120519.

[18] L. Kruitwagen, K.T. Story, J. Friedrich, L. Byers, S. Skillman, C. Hepburn, A global inventory of photovoltaic solar energy generating units, Nature. 598 (2021) 604–610. https://doi.org/10.1038/s41586-021-03957-7.

[19] E. Dogan, F. Seker, Determinants of CO2 emissions in the European Union: The role of renewable and non-renewable energy, Renew. Energy. 94 (2016) 429–439. https://doi.org/10.1016/j.renene.2016.03.078.

[20] T. Güney, Renewable energy, non-renewable energy and sustainable development, Int. J. Sustain. Dev. World Ecol. 26 (2019) 389–397. https://doi.org/10.1080/13504509.2019.1595214.

[21] P. Regnier, L. Resplandy, R.G. Najjar, P. Ciais, The land-to-ocean loops of the global carbon cycle, Nature. 603 (2022) 401–410. https://doi.org/10.1038/s41586-021-04339-9.

[22] Y. Uwiragiye, J. Wang, Y. Huang, L. Wu, J. Zhou, Y. Zhang, M. Chen, H. Jing, Y. Qian, A.S. Elrys, Y. Cheng, Z. Cai, M. Xu, S.X. Chang, C. Müller, Global Ecosystem Nitrogen Cycling Reciprocates Between Land-Use Conversion and Its Reversal, Glob. Chang. Biol. 30 (2024) 1–16. https://doi.org/10.1111/gcb.17537.

[23] S. Adams, E.K.M. Klobodu, A. Apio, Renewable and non-renewable energy, regime type and economic growth, Renew. Energy. 125 (2018) 755–767. https://doi.org/10.1016/j.renene.2018.02.135.

[24] S. Algarni, V. Tirth, T. Alqahtani, S. Alshehery, P. Kshirsagar, Contribution of renewable energy sources to the environmental impacts and economic benefits for sustainable development, Sustain. Energy Technol. Assessments. 56 (2023) 103098. https://doi.org/10.1016/j.seta.2023.103098.

[25] I. Dincer, Renewable energy and sustainable development: A crucial review,

Renew. Sustain. Energy Rev. 4 (2000) 157–175. https://doi.org/10.1016/S1364-0321(99)00011-8.

[26] Y. Majeed, M.U. Khan, M. Waseem, U. Zahid, F. Mahmood, F. Majeed, M. Sultan, A. Raza, Renewable energy as an alternative source for energy management in agriculture, Energy Reports. 10 (2023) 344–359. https://doi.org/10.1016/j.egyr.2023.06.032.

[27] T.Z. Ang, M. Salem, M. Kamarol, H.S. Das, M.A. Nazari, N. Prabaharan, A comprehensive study of renewable energy sources: Classifications, challenges and suggestions, Energy Strateg. Rev. 43 (2022) 100939. https://doi.org/10.1016/j.esr.2022.100939.

[28] P. Moriarty, D. Honnery, What is the global potential for renewable energy?, Renew. Sustain. Energy Rev. 16 (2012) 244–252. https://doi.org/10.1016/j.rser.2011.07.151.

[29] S. Roga, S. Bardhan, Y. Kumar, S.K. Dubey, Recent technology and challenges of wind energy generation: A review, Sustain. Energy Technol. Assessments. 52 (2022) 102239. https://doi.org/10.1016/j.seta.2022.102239.

[30] Z.M. Ghazi, S.W.F. Rizvi, W.M. Shahid, A.M. Abdulhameed, H. Saleem, S.J. Zaidi, An overview of water desalination systems integrated with renewable energy sources, Desalination. 542 (2022) 116063. https://doi.org/10.1016/j.desal.2022.116063.

[31] A.I. Osman, L. Chen, M. Yang, G. Msigwa, M. Farghali, S. Fawzy, D.W. Rooney, P.S. Yap, Cost, environmental impact, and resilience of renewable energy under a changing climate: a review, Environ. Chem. Lett. 21 (2023) 741–764. https://doi.org/10.1007/s10311-022-01532-8.

[32] P. McKendry, Energy production from biomass (part 1): Overview of biomass, Bioresour. Technol. 83 (2002) 37–46. https://doi.org/10.1016/S0960-8524(01)00118-3.

[33] C.B. Field, J.E. Campbell, D.B. Lobell, Biomass energy: the scale of the potential resource, Trends Ecol. Evol. 23 (2008) 65–72. https://doi.org/10.1016/j.tree.2007.12.001.

[34] S. V. Vassilev, D. Baxter, L.K. Andersen, C.G. Vassileva, An overview of the chemical composition of biomass, Fuel. 89 (2010) 913–933. https://doi.org/10.1016/j.fuel.2009.10.022.

[35] S. Wang, Z. Luo, 1. Biomass components and characteristics, 2016. https://doi.org/10.1515/9783110369632-003.

[36] J. Tivy, Biomass characteristics, Biogeography. (2019) 79–106. https://doi.org/10.4324/9781315845227-5.

[37] L. Brennan, A. Mostaert, C. Murphy, P. Owende, Phytochemicals from Algae, Biorefinery Co-Products Phytochem. Prim. Metab. Value-Added Biomass Process. (2012) 199–240. https://doi.org/10.1002/9780470976692.ch10.

[38] A. Raheem, W.A.K.G. Wan Azlina, Y.H. Taufiq Yap, M.K. Danquah, R. Harun, Thermochemical conversion of microalgal biomass for biofuel production, Renew. Sustain. Energy Rev. 49 (2015) 990–999. https://doi.org/10.1016/j.rser.2015.04.186.

[39] J. Yu, K. Maliutina, A. Tahmasebi, A review on the production of nitrogen-containing compounds from microalgal biomass via pyrolysis, Bioresour. Technol. 270 (2018) 689–701. https://doi.org/10.1016/j.biortech.2018.08.127.

[40] R. Yukesh Kannah, S. Kavitha, O. Parthiba Karthikeyan, E.R. Rene, G. Kumar, J. Rajesh Banu, A review on anaerobic digestion of energy and cost effective microalgae pretreatment for biogas production, Bioresour. Technol. 332 (2021) 125055. https://doi.org/10.1016/j.biortech.2021.125055.

[41] J. Lee, E.E. Kwon, Y.K. Park, Recent advances in the catalytic pyrolysis of microalgae, Catal. Today. 355 (2020) 263–271. https://doi.org/10.1016/j.cattod.2019.03.010.

[42] M. Al-Hammadi, M. Güngörmüşler, New insights into Chlorella vulgaris applications, Biotechnol. Bioeng. 121 (2024) 1486–1502. https://doi.org/10.1002/bit.28666.

[43] H.M.R. Abdel-Latif, S. El-Ashram, S. Yilmaz, M.A.E. Naiel, Z. Abdul Kari, N.K.A. Hamid, M.A.O. Dawood, J. Nowosad, D. Kucharczyk, The effectiveness of Arthrospira platensis and microalgae in relieving stressful conditions affecting

finfish and shellfish species: An overview, Aquac. Reports. 24 (2022) 101135. https://doi.org/10.1016/j.aqrep.2022.101135.

[44] T. Bridgwater, Biomass for energy, J. Sci. Food Agric. 86 (2006) 1755–1768. https://doi.org/10.1002/jsfa.2605.

[45] A. Kushwah, T.R. Reina, M. Short, Modelling approaches for biomass gasifiers: A comprehensive overview, Sci. Total Environ. 834 (2022) 155243. https://doi.org/10.1016/j.scitotenv.2022.155243.

[46] A.A. Adeleke, P.P. Ikubanni, S.S. Emmanuel, M.O. Fajobi, P. Nwachukwu, A.A. Adesibikan, J.K. Odusote, E.O. Adeyemi, O.M. Abioye, J.A. Okolie, A comprehensive review on the similarity and disparity of torrefied biomass and coal properties, Renew. Sustain. Energy Rev. 199 (2024) 114502. https://doi.org/10.1016/j.rser.2024.114502.

[47] Ö. Tezer, N. Karabağ, A. Öngen, C.Ö. Çolpan, A. Ayol, Biomass gasification for sustainable energy production: A review, Int. J. Hydrogen Energy. 47 (2022) 15419–15433. https://doi.org/10.1016/j.ijhydene.2022.02.158.

[48] A. Demirbas, Potential applications of renewable energy sources, biomass combustion problems in boiler power systems and combustion related environmental issues, Prog. Energy Combust. Sci. 31 (2005) 171–192. https://doi.org/10.1016/j.pecs.2005.02.002.

[49] H. Fatehi, W. Weng, Z. Li, X.S. Bai, M. Aldén, Recent development in numerical simulations and experimental studies of biomass thermochemical conversion, Energy and Fuels. 35 (2021) 6940–6963. https://doi.org/10.1021/acs.energyfuels.0c04139.

[50] Y.H. Chan, K.W. Cheah, B.S. How, A.C.M. Loy, M. Shahbaz, H.K.G. Singh, N.R. Yusuf, A.F.A. Shuhaili, S. Yusup, W.A.W.A.K. Ghani, J. Rambli, Y. Kansha, H.L. Lam, B.H. Hong, S.L. Ngan, An overview of biomass thermochemical conversion technologies in Malaysia, Sci. Total Environ. 680 (2019) 105–123. https://doi.org/10.1016/j.scitotenv.2019.04.211.

[51] Y. Wang, J.J. Wu, Thermochemical conversion of biomass: Potential future prospects, Renew. Sustain. Energy Rev. 187 (2023) 113754.

https://doi.org/10.1016/j.rser.2023.113754.

[52] T.Y.A. Fahmy, Y. Fahmy, F. Mobarak, M. El-Sakhawy, R.E. Abou-Zeid, Biomass pyrolysis: past, present, and future, Environ. Dev. Sustain. 22 (2020) 17–32. https://doi.org/10.1007/s10668-018-0200-5.

[53] Thermal Processing in an Inert Atmosphere (Pyrolysis), (2024) 861623.

[54] S. Wang, Z. Luo, Pyrolysis of biomass, 2017. https://doi.org/10.1515/9783110369632-009.

[55] R.W. Nachenius, F. Ronsse, R.H. Venderbosch, W. Prins, Biomass Pyrolysis, 1st ed., Elsevier Inc., 2013. https://doi.org/10.1016/B978-0-12-386505-2.00002-X.

[56] N. Aslan, Y. Cebeci, Application of Box-Behnken design and response surface methodology for modeling of some Turkish coals, Fuel. 86 (2007) 90–97. https://doi.org/10.1016/j.fuel.2006.06.010.

[57] M. Muthukumar, D. Mohan, M. Rajendran, Optimization of mix proportions of mineral aggregates using Box Behnken design of experiments, Cem. Concr. Compos. 25 (2003) 751–758. https://doi.org/10.1016/S0958-9465(02)00116-6.

[58] L. Wu, K.L. Yick, S.P. Ng, J. Yip, Application of the Box-Behnken design to the optimization of process parameters in foam cup molding, Expert Syst. Appl. 39 (2012) 8059–8065. https://doi.org/10.1016/j.eswa.2012.01.137.

[59] S.L.C. Ferreira, R.E. Bruns, H.S. Ferreira, G.D. Matos, J.M. David, G.C. Brandão, E.G.P. da Silva, L.A. Portugal, P.S. dos Reis, A.S. Souza, W.N.L. dos Santos, Box-Behnken design: An alternative for the optimization of analytical methods, Anal. Chim. Acta. 597 (2007) 179–186. https://doi.org/10.1016/j.aca.2007.07.011.

[60] P. Tripathi, V.C. Srivastava, A. Kumar, Optimization of an azo dye batch adsorption parameters using Box-Behnken design, Desalination. 249 (2009) 1273–1279. https://doi.org/10.1016/j.desal.2009.03.010.

[61] S.N. Nam, H. Cho, J. Han, N. Her, J. Yoon, Photocatalytic degradation of acesulfame K: Optimization using the Box–Behnken design (BBD), Process Saf. Environ. Prot. 113 (2018) 10–21. https://doi.org/10.1016/j.psep.2017.09.002.

[62] G.J. Swamy, A. Sangamithra, V. Chandrasekar, Response surface modeling and

process optimization of aqueous extraction of natural pigments from Beta vulgaris using Box-Behnken design of experiments, Dye. Pigment. 111 (2014) 64–74. https://doi.org/10.1016/j.dyepig.2014.05.028.

[63] X. Gong, B. Zhang, Y. Zhang, Y. Huang, M. Xu, Investigation on pyrolysis of low lipid microalgae chlorella vulgaris and dunaliella salina, Energy and Fuels. 28 (2014) 95–103. https://doi.org/10.1021/ef401500z.

[64] V. Vasudev, X. Ku, J. Lin, Combustion Behavior of Algal Biochars Obtained at Different Pyrolysis Heating Rates, ACS Omega. 6 (2021) 19144–19152. https://doi.org/10.1021/acsomega.1c02493.

[65] A. Raheem, V. Dupont, A.Q. Channa, X. Zhao, A.K. Vuppaladadiyam, Y.H. Taufiq-Yap, M. Zhao, R. Harun, Parametric Characterization of Air Gasification of Chlorella vulgaris Biomass, Energy and Fuels. 31 (2017) 2959–2969. https://doi.org/10.1021/acs.energyfuels.6b03468.

[66] M. Jin, Y.K. Oh, Y.K. Chang, M. Choi, Optimum Utilization of Biochemical Components in Chlorella sp. KR1 via Subcritical Hydrothermal Liquefaction, ACS Sustain. Chem. Eng. 5 (2017) 7240–7248. https://doi.org/10.1021/acssuschemeng.7b01473.

[67] S. DUMAN, B. KAYA, F. CAF, O. KOK, I. TUZUN, Magnetite Fe3O4 nanoparticles impregnated on Chlorella vulgaris microalgae: Its role in obtaining hydrogen from the sodium borohydride-hydrolysis, Algal Res. 84 (2024) 103745. https://doi.org/10.1016/j.algal.2024.103745.

[68] H. Saidi, Y.A. El Hadj Ali, A. Azzouz, A. Chraka, L. Bouzit, M. Stitou, Optimization and application of walnut shell-driver biochar for efficient removal of salicylic acid from wastewater: Experiment and theoretical study, Chem. Eng. Res. Des. 221 (2025) 22–36. https://doi.org/10.1016/j.cherd.2025.07.047.

[69] E.S.M. Al-Mashhadani, M.K.H. Al-Mashhadani, Utilization of Chlorella vulgaris after the Extraction Process in Wastewater Treatment as a Biosorption Material for Ciprofloxacin Removal, J. Ecol. Eng. 24 (2023) 1–15. https://doi.org/10.12911/22998993/159336.

[70] M.S. Islam, I. Maamoun, O. Falyouna, O. Eljamal, B.B. Saha, Arsenic removal

from contaminated water utilizing novel green composite Chlorella vulgaris and nano zero-valent iron, J. Mol. Liq. 370 (2023) 121005. https://doi.org/10.1016/j.molliq.2022.121005.

[71] N.O. Zhila, E.G. Kiselev, E.I. Shishatskaya, F.D.E. Ghorabe, A.S. Kazachenko, T.G. Volova, Comparative study of the synthesis of polyhydroxyalkanoates by cyanobacteria Spirulina platensis and green microalga Chlorella vulgaris, Algal Res. 85 (2025) 103826. https://doi.org/10.1016/j.algal.2024.103826.

[72] K. Azizi, M. Keshavarz Moraveji, H. Abedini Najafabadi, Characteristics and kinetics study of simultaneous pyrolysis of microalgae Chlorella vulgaris, wood and polypropylene through TGA, Bioresour. Technol. 243 (2017) 481–491. https://doi.org/10.1016/j.biortech.2017.06.155.

[73] L. Chen, Z. Yu, S. Fang, M. Dai, X. Ma, Co-pyrolysis kinetics and behaviors of kitchen waste and chlorella vulgaris using thermogravimetric analyzer and fixed bed reactor, Energy Convers. Manag. 165 (2018) 45–52. https://doi.org/10.1016/j.enconman.2018.03.042.

[74] M.J.B. Fong, A.C.M. Loy, B.L.F. Chin, M.K. Lam, S. Yusup, Z.A. Jawad, Catalytic pyrolysis of Chlorella vulgaris: Kinetic and thermodynamic analysis, Bioresour. Technol. 289 (2019) 121689. https://doi.org/10.1016/j.biortech.2019.121689.

[75] C.E. Figueira, P.F. Moreira, R. Giudici, Thermogravimetric analysis of the gasification of microalgae Chlorella vulgaris, Bioresour. Technol. 198 (2015) 717–724. https://doi.org/10.1016/j.biortech.2015.09.059.

[76] C. Chen, X. Ma, Y. He, Co-pyrolysis characteristics of microalgae Chlorella vulgaris and coal through TGA, Bioresour. Technol. 117 (2012) 264–273. https://doi.org/10.1016/j.biortech.2012.04.077.

[77] A. Raheem, S. Sivasangar, W.A.K.G. Wan Azlina, Y.H. Taufiq Yap, M.K. Danquah, R. Harun, Thermogravimetric study of Chlorella vulgaris for syngas production, Algal Res. 12 (2015) 52–59. https://doi.org/10.1016/j.algal.2015.08.003.

[78] M.A. Kassim, K. Kirtania, D. De La Cruz, N. Cura, S.C. Srivatsa, S. Bhattacharya,

Thermogravimetric analysis and kinetic characterization of lipid-extracted Tetraselmis suecica and Chlorella sp., Algal Res. 6 (2014) 39–45. https://doi.org/10.1016/j.algal.2014.08.010.

[79] L. Chen, Z. Yu, J. Liang, Y. Liao, X. Ma, Co-pyrolysis of chlorella vulgaris and kitchen waste with different additives using TG-FTIR and Py-GC/MS, Energy Convers. Manag. 177 (2018) 582–591. https://doi.org/10.1016/j.enconman.2018.10.010.

[80] C. Zhang, S.H. Ho, W.H. Chen, R. Wang, Comparative indexes, fuel characterization and thermogravimetric- Fourier transform infrared spectrometer-mass spectrogram (TG-FTIR-MS) analysis of microalga Nannochloropsis Oceanica under oxidative and inert torrefaction, Energy. 230 (2021) 120824. https://doi.org/10.1016/j.energy.2021.120824.

[81] D. López-González, M. Fernandez-Lopez, J.L. Valverde, L. Sanchez-Silva, Pyrolysis of three different types of microalgae: Kinetic and evolved gas analysis, Energy. 73 (2014) 33–43. https://doi.org/10.1016/j.energy.2014.05.008.

[82] W.H. Chen, K.Y. Ho, R. Aniza, A.K. Sharma, A. Saravanakumar, A.T. Hoang, A review of noncatalytic and catalytic pyrolysis and co-pyrolysis products from lignocellulosic and algal biomass using Py-GC/MS, J. Ind. Eng. Chem. 134 (2024) 51–64. https://doi.org/10.1016/j.jiec.2024.01.020.

[83] W. Kong, B. Shen, J. Ma, J. Kong, S. Feng, Z. Wang, L. Xiong, Pyrolysis of Spirulina platensis, Tetradesmus obliquus and Chlorella vulgaris by TG-FTIR and Py-GC/MS: Kinetic analysis and pyrolysis behaviour, Energy. 244 (2022) 123165. https://doi.org/10.1016/j.energy.2022.123165.

LIST OF PUBLICATIONS ABOUT THE THESIS SUBJECT BEING PREPARED

1. Papers Published on Science Citation Expanded Index Journal

S.Polat & Ö.F. Kılıç, Pyrolysis of *Chlorella vulgaris*: Kinetic Analysis, Advanced Characterization, and Bio-Oil Optimization, Submitted to Journal of Environmental Chemical Engineering.

2. Presented Announcements

1. Ö.F. Kılıç & S. Polat (2025). Mikroalglerin Termal Analiz Yöntemiyle Piroliz Kinetiğinin İncelenmesi, I. Ulusal Enerji Dönüşümü ve Sürdürülebilirlik Konferansı (EDSK'25). (Oral presentation)

2. S. Polat & Ö.F. Kılıç (2025). Thermal Decomposition Behavior of *Chlorella Vulgaris* via TGA-FTIR Analysis, International Conference on Energy Systems (ICES-25). (Oral presentation).

3. S. Polat & Ö.F. Kılıç (2025). Thermal Analysis-Based Investigation of the Pyrolysis Kinetics of *Spirulina platensis,* 6th International Eurasian Conference on Science, Engineering and Technology (EurasianSciEnTech 2025). (Oral presentation).

4. S. Polat & Ö.F. Kılıç (2025). *Chlorella vulgaris* Mikroalgleri için Piroliz Sürecinin Deneysel Optimizasyonu, 16. Ulusal Kimya Mühendisliği Kongresi (UKMK-16). (Oral presentation).

CURRICULUM VITAE

Ömer Faruk KILIÇ

EDUCATION

Master of Science	Marmara University (2024 – November 2025) Chemical Engineering (GPA: 4.00/4.00)
Bachelor of Science	Bahçeşehir University (2018 – 2022) Energy Systems Engineering
High School	Şehremini Anatolian High School (2014 – 2018)

WORK EXPERIENCE

Dec 2024 -	CK Enerji A.Ş. Senior Energy Balancing Specialist
Aug 2022 - Dec 2024	VTC Enerji A.Ş. Energy Trading Specialist
Jan 2022 - Aug 2022	Yıldırım Energy Holding Assistant Energy Trading Specialist
Feb 2021 - Dec 2021	Odaş Enerji A.Ş. Assistant Energy Trading Specialist

LANGUAGE

Turkish (Native), English (Native)